RESEARCH ARTICLE | MAY 11 2026

Main phase transition of hydroperoxidized SOPC bilayers

Special Collection: Festschrift in honor of Kurt Kremer: Computational Polymer Science and Soft Matter Physics

Eulalie Lafarge ; Sifre van Teeffelen ; André P. Schroder ; Pierre Muller ; Fabrice Thalmann ; Yann Bretonnière; Lorenzo Metilli ; Apostolos Vagias; Léo Corne ; Carlos M. Marques

J. Chem. Phys. 164, 185101 (2026)
https://doi.org/10.1063/5.0323202

The Journal of Chemical Physics ARTICLE pubs.aip.org/aip/jcp

Main phase transition of hydroperoxidized SOPC bilayers

Cite as: J. Chem. Phys. 164, 185101 (2026); doi: 10.1063/5.0323202
Submitted: 16 January 2026 • Accepted: 20 April 2026 •
Published Online: 11 May 2026

Eulalie Lafarge,[1] Sifre van Teeffelen,[2] André P. Schroder,[3] Pierre Muller,[1] Fabrice Thalmann,[1] Yann Bretonnière,[2] Lorenzo Metilli,[4] Apostolos Vagias,[5] Léo Corne,[2] and Carlos M. Marques[2,a)]

AFFILIATIONS

[1] Institut Charles Sadron, CNRS UPR22 & Université de Strasbourg, Strasbourg 67000, France
[2] University of Lyon, ENS-Lyon, CNRS UMR 5182, Chem. Lab, Lyon 69342, France
[3] CNRS, INSA Lyon, LaMCoS, UMR5259, Villeurbanne 69621, France
[4] Laboratoire Leon Brillouin, UMR12 CEA-CNRS, Gif-sur-Yvette 91191, France
[5] ILL, Institut Laue-Langevin, 71 Avenue des Martyrs, Grenoble 38042, France

Note: This paper is part of the JCP Festschrift in Honor of Kurt Kremer.
[a)] **Author to whom correspondence should be addressed:** carlos.marques@ens-lyon.fr

ABSTRACT

Lipid hydroperoxidation significantly changes membrane biophysical properties, yet its effect on the main phase transition of unsaturated phospholipids remains unclear. Here, we investigate how hydroperoxidation of 1-stearoyl-2-oleoyl-sn-glycero-3-phosphocholine (SOPC) influences its phase behavior. Bilayers composed of SOPC and increasing fractions of hydroperoxidized SOPC (SOPC-OOH) were analyzed using differential scanning calorimetry, the band shift of the new solvatochromic probe A10, and Laurdan generalized polarization fluorescence. The incorporation of hydroperoxidized acyl chains perturbed membrane thermodynamics, revealing a complex phase-transition landscape governed by the interplay between acyl-chain ordering and the spatial distribution of –OOH groups. These results highlight the sensitivity of lipid phase behavior to oxidative modifications at the molecular level and provide new insights into how lipid peroxidation modulates membrane organization in cellular and biomimetic systems.

I. INTRODUCTION

Biological membranes are complex, dynamic assemblies of lipids and other molecules whose physical properties are central to cellular function.[1,2] Among the various determinants of membrane behavior, lipid composition plays a crucial role in modulating membrane fluidity, permeability, and thermodynamic state. Phosphatidylcholines (PCs), as a major class of cellular phospholipids, have been extensively studied to elucidate fundamental aspects of membrane thermodynamics.[3] Membrane fluidity is vital for cellular metabolism, underpinning key processes such as nutrient transport, signal transduction, and enzymatic activity within lipid bilayers. This essential fluidity is conferred by the presence of unsaturated acyl chains, which introduce structural kinks that disrupt tight packing and lower the gel-to-fluid (L_β-to-L_α) crystalline phase transition temperature. However, the same unsaturations that promote fluidity also render lipids particularly susceptible to oxidative damage. Reactive oxygen species readily abstract allylic hydrogens, initiating peroxidation and leading to the formation of lipid hydroperoxides.[4] Lipid peroxidation, particularly of membrane phospholipids, is implicated under a wide range of pathological conditions, including neurodegenerative diseases, inflammation, and aging.[5]

Oxidized phospholipids are known to alter bilayer packing and hydration, but quantitative biophysical data on the effects of well-defined oxidation products remain limited. In particular, mixtures of native and oxidized lipids provide a more biologically relevant model for understanding membrane behavior under oxidative stress. In this context, 1-stearoyl-2-oleoyl-sn-glycero-3-phosphocholine (SOPC) offers an especially advantageous model lipid for studying bilayer phase transitions. Structurally, SOPC closely resembles the widely studied POPC, featuring a phosphocholine head group with one saturated and one monounsaturated acyl chain, similar to the most abundant phosphatidylcholine species in mammalian membranes.[6] Unlike POPC, however, SOPC exhibits

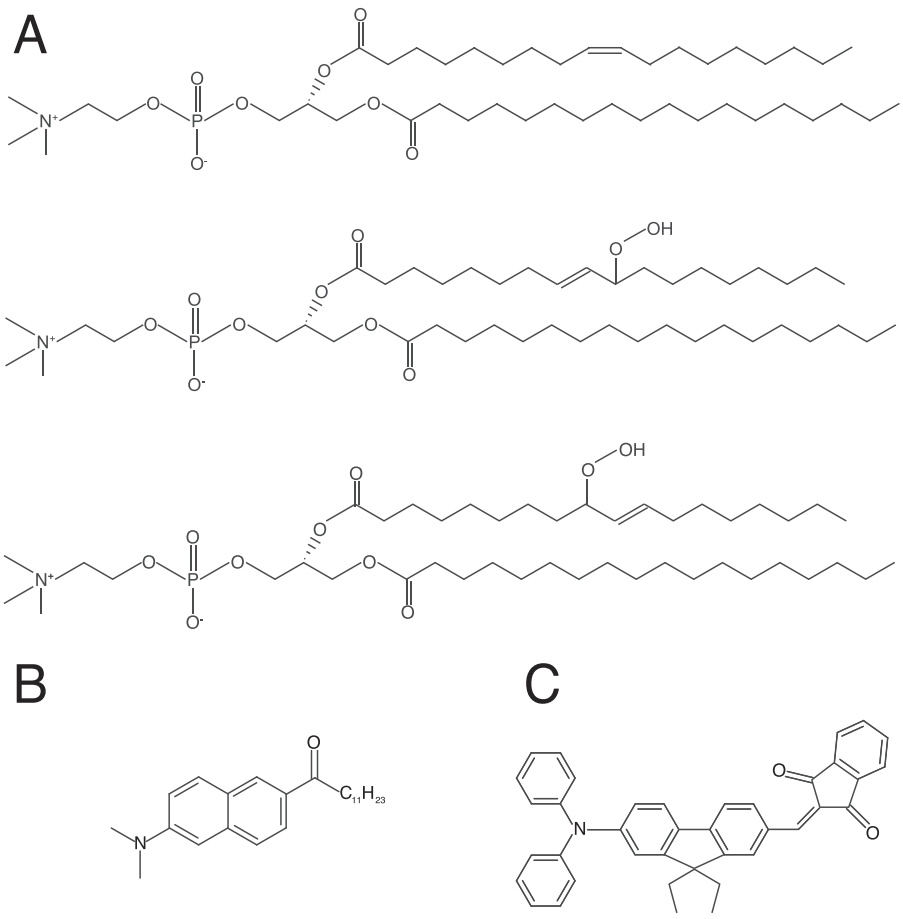

FIG. 1. Chemical structures of molecules used in this study. (a) SOPC and SOPC–OOH. Note the organic hydroperoxide group insertion at either the 9′ or the 10′ position and the trans nature of the unsaturated bond in the hydroperoxidized tails. (b) Laurdan. (c) A10.

a main transition temperature (T_m) well above 0 °C, experimentally determined around 279 K (~6 °C),[7] enabling thermotropic properties to be probed under convenient laboratory conditions without the complications of freezing.

Here, we investigated the thermodynamic behavior of binary mixtures of SOPC and its hydroperoxidized form SOPC–OOH, shown in Fig. 1(a), to assess how oxidative modification affects membrane phase transitions. Using differential scanning calorimetry (DSC), we quantified changes in the main phase transition temperature, transition enthalpy, and cooperativity as a function of oxidized lipid content. These thermodynamic parameters provide insight into how peroxidation disrupts acyl chain ordering and lipid–lipid interactions within the bilayer. To complement the calorimetric analysis, we characterized the thickness of the membranes by small angle neutron scattering (SANS) and employed steady-state fluorescence spectroscopy using two environment-sensitive probes: Laurdan [Fig. 1(b)], a well-established marker of membrane phase and hydration,[8,9] and A10 [Fig. 1(c)], a recently developed solvatochromic probe applied here for the first time to monitor membrane changes.[10] Together, these complementary techniques provide a detailed picture of how oxidation of a single lipid species perturbs the structural and thermodynamic properties of model membranes.

II. MATERIALS AND METHODS

A. Materials

1-stearoyl-2-oleoyl-sn-glycero-3-phosphocholine (SOPC, 18:0-18:1 PC) and 1-(6-(dimethylamino)naphthalen-2-yl)dodecan-1-one (Laurdan) were purchased from Avanti Polar Lipids. SOPC was dissolved in chloroform to prepare a 50 mg/ml stock solution and stored at −20 °C. Deuterated methanol (MeOD, 99.8%) was obtained from Eurisotop. Methylene blue hydrate (MB, $C_{16}H_{18}ClN_3S{\cdot}xH_2O$) was purchased from Alfa Aesar and prepared as a 50 mM stock solution in MeOD. The solvatochromic dye A10 was synthesized as previously described by Zheng *et al.*[10]

B. SOPC–OOH synthesis

Hydroperoxidation of SOPC was carried out using methylene blue (MB) as a photosensitizer. SOPC (10 mg, 0.013 mmol) was dissolved in MeOD (5 ml), and MB (50 μl of a 50 mM stock solution) was added to obtain a final MB concentration of 50 μM. The solution was irradiated with red light (λ = 656 nm, P = 600 W · m^{-2}) for 10 min under continuous oxygen bubbling and magnetic stirring to induce lipid hydroperoxidation. Removal of MB was achieved by dialysis. In particular, 1 ml of the hydroperoxidized lipid solution

was dried by rotary evaporation and the resulting film was rehydrated in distilled water (2 ml). The dispersion was sonicated for 5 min and transferred into a cellulose ester dialysis membrane (molecular weight cutoff of 3.5–5 kDa), followed by dialysis against distilled water. After dialysis, the sample was freeze-dried and redissolved in MeOD. The lipids were characterized by ^{1}H NMR spectroscopy before and after hydroperoxidation, as well as after freeze-drying. Samples were stored at −20 °C until further use.

C. Liposome preparation for DSC measurements

Liposomes were prepared from different fractions of oxidized and non-oxidized lipids, corresponding to varying degrees of hydroperoxidation, with molar ratio ranging from 0% to 100% SOPC–OOH. Each lipid sample was prepared by drying 250 μl of a 10 mg/ml solution in MeOD under reduced pressure to form a thin lipid film. The dry film was rehydrated with 250 μl of Milli-Q water. Gentle hydration was carried out at room temperature until complete dispersion of the lipid film was achieved. The resulting suspension was vortexed for 1 minute (Top Mix FB15024, Fisher Scientific) and sonicated for 15 minutes in a water bath sonicator. This process yielded liposomes of various sizes and degrees of lamellarity.

D. DSC measurements and analysis

Differential scanning calorimetry (DSC) was performed using a μ-DSC (MC DSC, TA Instruments) calibrated with a pure sapphire standard. Each measurement cell was filled with 250 μl of the prepared liposome suspension. The reference cell was filled with Milli-Q water, and sample and reference cell masses were equilibrated by volume adjustment with water, reaching a final concentration of 7 mg/ml. Cooling scans were performed, from 20 to −12 °C, at a constant scan rate of 0.25 °C/min. Prior to each scan, the temperature was held isothermally to ensure thermal equilibrium. Thermograms were acquired using MCDSCrun software. The baseline-subtracted, normalized DSC traces (J/s/mol) were integrated over time to compute ΔH values. For samples where a single transition was identified, a trace fit was performed by considering the transition function $g(T) = 1/\Delta T \times \exp\{-(T - T_m)/\Delta T\})/(1 + \exp\{-(T - T_m)/\Delta T\})^2$[23] and the corresponding convolution of $g(T) \times \Delta H$ with an instrument response $R(T) = \exp\{-T/w_T\}/w_T$, providing the transition temperature T_m, the width of the transition ΔT, and the response delay of the calorimeter w_T. When two transition processes were identified, the fit was performed with a weighted contribution of $g^1(T)$ and $g^2(T)$ providing values for T_m^1 and T_m^2, the widths of the two transitions ΔT_1 and ΔT_2, and the response delay of the calorimeter w_T. We have also performed heating DSC scans with comparable results (data not reported). In addition, faster scans upon cooling and heating were acquired for all samples as a preparatory step before the final acquisition at the slowest practically feasible rate.

E. Liposome preparation for spectroscopic and SANS measurements

Liposomes were prepared from 1 mg of total lipid, consisting of mixtures of SOPC and its hydroperoxidized derivative (SOPC–OOH) at defined molar ratios of 0%, 25%, 50%, 75%, and 100% SOPC–OOH. For fluorescent labeling, A10 was incorporated at a molar ratio of 1:200, relative to the total lipid, and Laurdan at 1:500. Lipids and probes were co-dissolved in chloroform, and the solvent was removed under reduced pressure by rotary evaporation to form thin lipid films. The films were hydrated with 3 ml of distilled water and sonicated in a bath for 5 min. A10-labeled liposomes were further processed by tip sonication at 10% amplitude with pulsed cycles (10 s on, 10 s off) for a total on-time of 1 min. For small-angle neutron scattering (SANS) measurements, liposomes were prepared in D_2O instead of H_2O. Samples were stored at 4 °C until use.

F. A10 measurements and analysis

Liposomes labeled with the A10 solvatochromic dye were diluted fivefold in Milli-Q water and placed in a quartz cuvette for fluorescence measurements. Emission spectra were recorded using an AvaSpec-ULS2048 × 64 spectrometer (Avantes), coupled with a TC1 temperature controller and probe (Quantum Northwest) for precise thermal regulation. Excitation was set at 455 nm, with an integration time of 1 s, and each spectrum was averaged over 10 accumulations. Spectra were acquired at 1 °C intervals while the sample temperature was decreased from 15 °C to the frozen state and subsequently increased back to 15 °C. During measurements, the sample was continuously stirred with a magnetic stirrer, and a gentle argon flow was applied to the sample chamber to prevent condensation on the cuvette. The emission peak was refined by fitting a Gaussian function to the spectral region ±20 nm around the detected maximum. Temperature-dependent data were analyzed to determine the fluid fraction $\alpha(T) = \int_{-\infty}^{T} g(T')dT'$, also providing the transition temperature T_m and the width of the transition ΔT as probed by the solvatochromic sensitivity of A10.

G. Laurdan measurements and analysis

Fluorescence measurements of Laurdan-labeled liposomes were performed as described for A10-labeled liposomes, except that Laurdan-labeled liposomes were diluted threefold and excited at 365 nm. Spectra were corrected for sample scattering using the form $A + (B/\lambda)^4$. Generalized polarization (GP) was calculated in a standard manner from $GP = (I_{440} - I_{490})/(I_{440} + I_{490})$, where I_{440} and I_{490} are the emission intensities at 440 and 490 nm, respectively. Temperature-dependent values of GP from Laurdan-labeled liposomes were fitted using the same method as for the probe A10, providing another independent measurement of the transition temperature T_m and the width of the transition ΔT as probed by Laurdan.

H. SANS measurements

Liposomes with a concentration of 1 mg/ml were prepared for three samples: (i) pure SOPC, (ii) a mixture of 50% SOPC and 50% hydroperoxidized SOPC, and (iii) a fully hydroperoxidized SOPC. The samples were measured using small-angle neutron scattering (SANS) at the instrument SAM,[11] operated by the Laboratoire Léon Brillouin at ILL-Institute Laue Langevin (Grenoble, France). The samples were filled into flat quartz cells with a 1 mm optical path length and measured at six temperatures ranging between $T = 4$ °C and $T = 14.8$ °C using a refrigerated bath circulator.

A range of scattering vectors $q = 5 \times 10^{-3}$–0.5 Å^{-1} was covered using neutrons at $\lambda = 6$ Å, selected using a helical velocity selector

with wavelength resolution $\Delta\lambda/\lambda = 0.1$, and three different sample-to-detector distances (0.9, 2.25, and 6.7 m). The incoming beam was collimated through a square source (30×30 mm^2) and a rectangular aperture of 7×10 mm^2 over collimation lengths of 2.5, 5 and 9 m, respectively. Two-dimensional raw patterns were recorded using a 64×64 cm ^{23}He position-sensitive detector (256×128 pixels). They were then corrected for electronic and ambient background, empty cell scattering, detector uniformity, and beam transmissions, before being scaled to absolute cross sections, via the attenuated direct beam intensity, measured for each instrument configuration, and radially averaged using GRASP software.[12]

A measure of the membrane bilayer thickness was determined from the data by analyzing the linear region of the $\ln[q^2 I(q)]$ vs q^2 plot. In this $q-$ region, one extracts the radius of gyration r_g of the membrane thickness, which is the second moment of the scattering length density (SLD) measured vertically to the membrane.[13] Note that this is a model-independent determination, contrary to more complex fitting procedures that assume a spherical liposome shape and some liposome size-distribution. To follow the conventions often used in the literature, we give the thickness of the membrane as $h = r_g\sqrt{12}$, which would be the thickness of a membrane with a step-function SLD. An example of this procedure is given in Fig. S1 of the supplementary material.

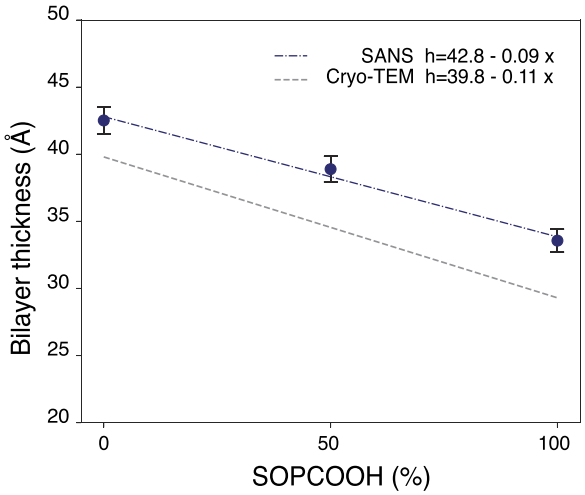

FIG. 2. Membrane bilayer thickness as a function of hydroperoxidation degree. Data points with the vertical error bars represent the SANS-derived thickness, including composed uncertainties from the linear fits. The blue dashed–dotted line is a linear fit through the SANS data points, while the gray dashed line shows the corresponding Cryo-TEM reference line, as previously reported in Ref. 14.

III. RESULTS

To investigate the effects of lipid oxidation on membrane properties and main phase transition, we employed three complementary experimental techniques: differential scanning calorimetry (DSC) as well as Laurdan and A10 fluorescence spectroscopy. Each method provides insight into distinct aspects of membrane behavior, including phase transition temperature, enthalpy, lipid packing, and bilayer polarity. As a preliminary investigation of the hydroperoxidized membrane, small-angle neutron scattering (SANS) was used to obtain direct structural information, providing complementary data on bilayer thickness and its variation with increasing hydroperoxidation.

A. SANS

Figure 2 shows the membrane bilayer thickness as a function of hydroperoxidation fraction for a temperature range above the main transition from the acquired SANS data. No significant data could be acquired for temperatures below T_m due to D_2O freezing. While the bilayer thickness is nearly independent of T in the T range explored (also see Fig. S2 in the supplementary material), a clear decreasing trend is observed with increasing hydroperoxidation, consistent with previous measurements using Cryo-TEM by Lafarge and coworkers;[14] a linear fit derived from their observations is also shown in the figure. For SANS, the membrane bilayer thickness in Å follows $h = 42.8 - 0.09x$, while the Cryo-TEM reference line also in Å follows $h = 39.8 - 0.10x$, where x is the hydroperoxidation percentage. Considering the percentage change from pure SOPC to fully hydroperoxidized SOPC, the thickness measured by SANS shows a decrease of ~21%, while Cryo-TEM shows a decrease of ~26%. The 50:50 mixture falls between the extremes, confirming the approximately linear thinning of the bilayer with increasing hydroperoxide content. Complete SANS curves for all three samples measured at different temperatures are provided in Figs. S3–S5 in the supplementary material.

B. DSC

DSC was used to assess the thermodynamic behavior of liposomes composed of SOPC and increasing molar fractions of its hydroperoxidized form, SOPC–OOH. Representative cooling-scan thermograms at different oxidation levels are shown in Fig. 3(a), while the full set of DSC traces is provided in Figs. S6–S12 of the supplementary material. During the fluid-to-gel phase transition upon cooling, lipid acyl chains reorganize to form ordered structures. Pure SOPC exhibited a symmetric main transition peak in a T-range between ~2–6 °C. As the SOPC–OOH content increased, the position of the peak shifted to lower temperatures down to around −4 °C for liposomes of hydroperoxidized lipids. At higher oxidation levels, the transition peak broadened and became asymmetric, possibly reflecting phase separation between SOPC and SOPC–OOH or the presence of distinct lipid environments within the bilayer. The thermogram of pure SOPC–OOH also displayed a distinct asymmetry and could be deconvoluted into two components, suggesting a two-step transition process. In addition to changes in transition temperature and peak shape, the enthalpy of the transition (ΔH) varied as a function of SOPC–OOH content [Fig. 3(b)]. At low oxidation levels, ΔH decreased slightly by 15%, suggesting a modest reduction in the number of lipid molecules participating in the cooperative phase transition. Surprisingly, at higher oxidation levels, the enthalpy increased, reaching ~1.5 times the value observed for pure SOPC: $\Delta H_{\text{SOPC-OOH}} \approx 1.5\ \Delta H_{\text{SOPC}}$. This trend suggests that highly oxidized membranes may undergo more complex phase transitions, potentially involving additional hydrogen bonding from –OOH groups.

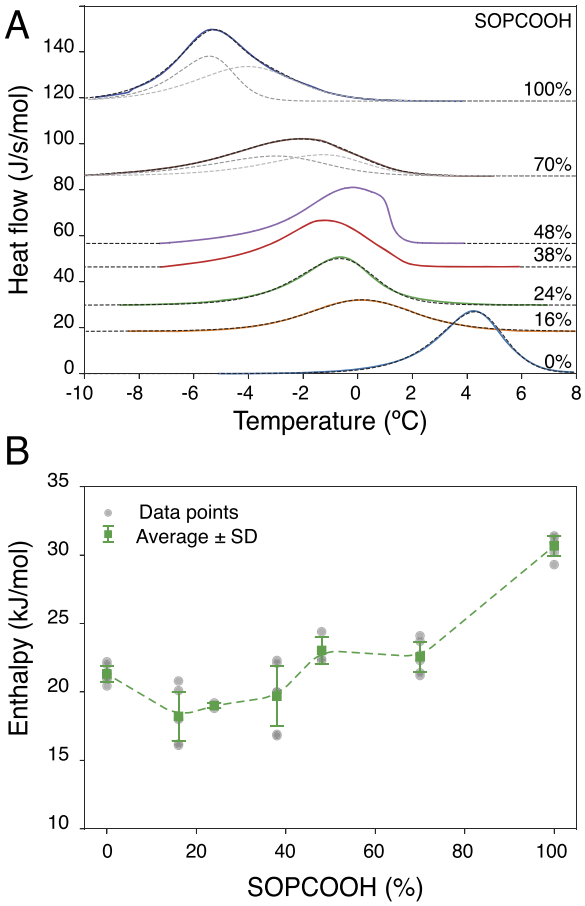

FIG. 3. (a) Typical DSC traces under cooling at 0.25 °C/min of SOPC/SOPC–OOH mixtures. For clarity, trace baselines are vertically displaced proportionally to SOPC–OOH content. Fits are also displayed for transitions where one or two transition processes can be identified. (b) Corresponding average phase transition enthalpies of SOPC/SOPC–OOH mixtures with standard deviation (SD).

C. A10

Peak wavelength (λ_{max}) values were measured as a function of temperature for liposomes containing increasing fractions of oxidized SOPC (SOPC–OOH), as shown in Fig. 4. Fluorescence intensity spectra at selected temperatures are provided in Figs. S13–S17 of the supplementary material. The solvatochromic probe A10 exhibits a temperature-dependent redshift of its emission maximum (λ_{max}) with increasing solvent polarity. Due to its size and hydrophobicity, A10 is expected to be deeply embedded within the bilayer chains. Across all samples, λ_{max} initially decreased upon cooling with a similar slope. At the main phase transition, λ_{max} increased, reflecting changes in bilayer polarity and/or viscosity. This increase took place at 4–6 °C for pure SOPC. With higher SOPC–OOH fractions, the transition shifted to lower temperatures.

D. Laurdan

Laurdan generalized polarization (GP) values were determined as a function of temperature for liposomes containing increasing

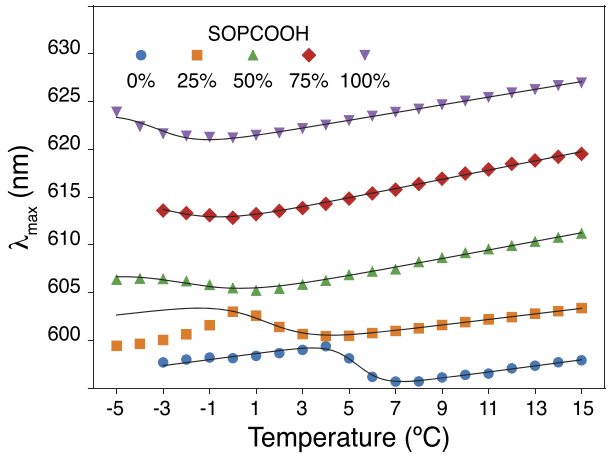

FIG. 4. A10 peak wavelength variation with temperature for lipid membranes assembled from mixtures of SOPC and SOPC–OOH. The data are offset vertically by 5 nm with pure SOPC unshifted and each subsequent sample shifted upward incrementally for clarity.

fractions of oxidized SOPC (SOPC–OOH), as shown in Fig. 5. Here also, fluorescence intensity spectra at different temperatures are provided in Figs. S18–S22 of the supplementary material. Laurdan localizes under the headgroup region of phospholipids, where it is particularly sensitive to changes in polarity and interfacial hydration.[15] Across all samples, GP increased upon cooling, consistent with a decrease in local polarity and hydration around the probe. The sharper increase in GP indicates the gel-to-fluid main phase transition. For pure SOPC, GP increased sharply around 5–6 °C. Incorporation of SOPC–OOH shifted the transition to lower temperatures for samples with 25% and 50% hydroperoxidation, after which this temperature appeared to plateau. The overall GP change during the transition decreased with increasing oxidation level, suggesting that oxidation disrupts membrane

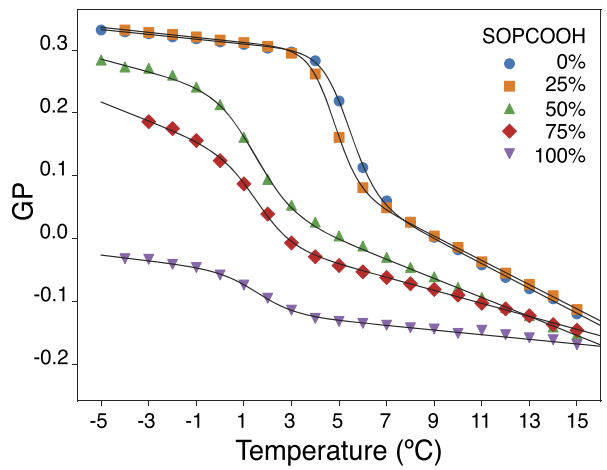

FIG. 5. Laurdan generalized polarization variation with temperature for lipid membranes assembled from mixtures of SOPC and SOPC–OOH.

cooperativity and reduces the extent of ordering achievable in the gel phase.

IV. DISCUSSION AND CONCLUSIONS

Our results reveal how lipid hydroperoxidation affects SOPC membrane structure and phase behavior, as evidenced by DSC, Laurdan GP, and A10 fluorescence measurements.

A. Phase transition profiles

Figure 6 compares normalized phase transition functions (i.e. $g(T)/\int_{-\infty}^{\infty} g(T)dT$) of SOPC membranes with increasing lipid hydroperoxidation (0%–100% –OOH), as determined from Laurdan, A10, and DSC measurements. The transition functions show that increasing oxidation systematically shifts the main phase transition toward lower temperatures and broadens the transition profile. At 70% and 100% SOPC–OOH, the DSC transitions could be fitted with two components, suggesting either multiple structural states or a two-stage transition process, in which –OOH group repositioning and acyl-chain ordering occur as separate events.

B. Phase transition temperatures

As summarized in Fig. 7, the transition temperatures extracted from A10, Laurdan, and DSC data agree closely for pure SOPC. With increasing oxidation, all probes show a progressive decrease in transition temperature. The shift for Laurdan levels off about 50% SOPC–OOH, suggesting that the bilayer interfacial region reaches a structurally saturated regime where additional oxidation produces less incremental destabilization. Notably, the transition temperature reported by A10 is consistently lower than that reported by Laurdan in all membranes with a finite fraction of hydroperoxidized SOPC. This difference likely arises because of a difference in location of the probes in the bilayer, suggesting that the region of the hydrophobic core undergoes ordering changes at lower temperatures than the interfacial region.

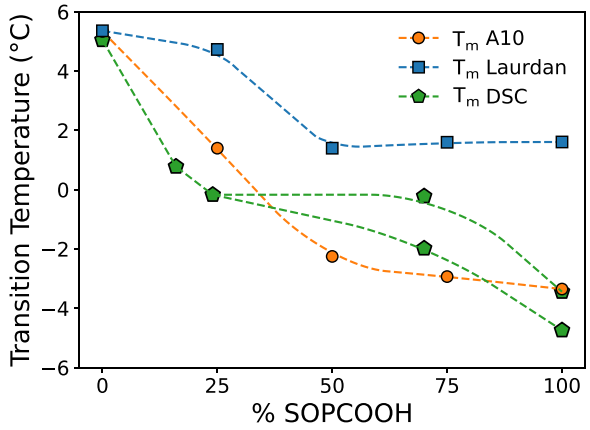

FIG. 7. Transition temperatures extracted from A10, Laurdan, and DSC data. Note that the DSC data at 70% and 100% SOPCOOH was fitted with two components, corresponding to two extracted transition temperatures.

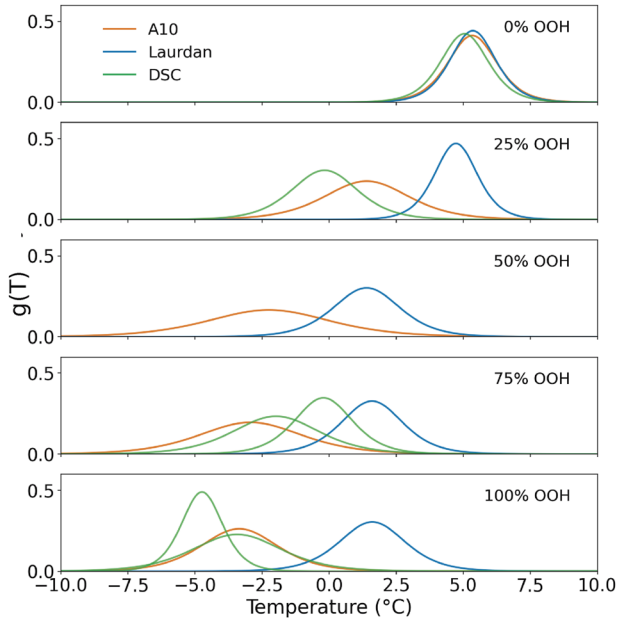

FIG. 6. Comparison of phase transition profiles of SOPC membranes with increasing lipid hydroperoxidation (0%–100% –OOH) based on Laurdan and A10 fluorescence and DSC data. Each panel shows the derivative of sigmoid fits as a function of temperature, normalized to area. Laurdan (blue), A10 (orange), and DSC (green) curves provide insight into the phase transition temperatures (T_0) and widths (ΔT).

C. Bilayer properties in gel and fluid phases

The comparison of Laurdan GP and A10 λ_{max} values at representative gel (−3 °C) and fluid (15 °C) temperatures (Fig. 8) provides

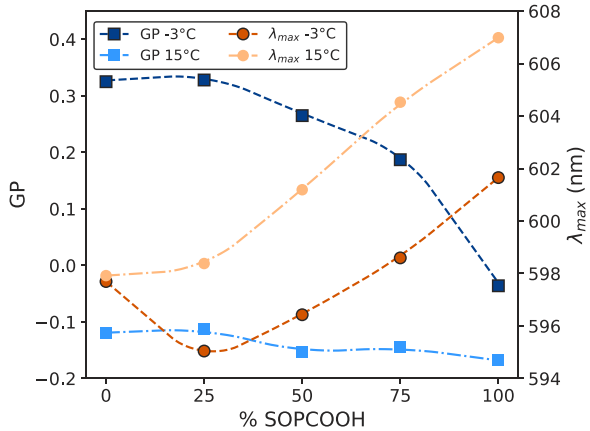

FIG. 8. Laurdan GP (blue, left axis) and A10 λ_{max} (orange, right axis) values in the gel (−3 °C) and fluid (15 °C) phases of SOPC membranes containing increasing fractions of oxidized lipid (SOPC–OOH). The fluid-phase GP remains nearly constant across oxidation levels, while the gel-phase GP decreases markedly beyond 25% –OOH. The λ_{max} values show a clear red shift with increasing oxidation above 25%. For highly oxidized samples, the λ_{max} values at −3 °C may partially overlap with the phase transition, which could influence the apparent gel-phase λ_{max}.

additional insight into how lipid hydroperoxidation modifies bilayer polarity and packing. The nearly constant GP values in the fluid phase indicate that once the bilayer is fully fluid, oxidation no longer significantly alters membrane interfacial hydration. In contrast, the pronounced decrease in gel-phase GP beyond roughly 25% SOPC–OOH reflects a progressive loss of lipid order and enhanced water or –OOH group presence into the interfacial region.

The λ_{max} values derived from the A10 probe show a complementary trend: they remain nearly unchanged in the gel phase up to 25% oxidation but display a clear redshift in the fluid phase above this level. This suggests that once a critical concentration of hydroperoxide groups is reached, the polarity experienced by A10 within the bilayer interior increases substantially. Together, these observations might imply that below about 25% oxidation, most –OOH groups are oriented toward the membrane surface, where they can interact with interfacial water (state 1 in Fig. 9), while above 25% –OOH groups also populate the core of the bilayer. This has been predicted in several studies using numerical simulations. Pioneering studies have shown that hydroperoxide lipids have higher propensity to form hydrogen bonds with water, suggesting that –OOH groups reside in the proximity of the lipid headgroup region.[16,17] Such non-uniformity of the –OOH distribution along the z-direction (the normal to the bilayer plane), for a given oxidation level, also depends on the position of the –OOH group along the unsaturated chain itself, a situation typical of partially oxidized polyunsaturated chains.[18] In the particular case of POPC, a monounsaturated phospholipid similar to SOPC, a detailed study of the –OOH group distribution along the membrane z-direction has shown that only above 25% oxidation does a substantial fraction of the –OOH populate the inner core of the bilayer[19] (Fig. 9 shows illustrations in very good agreement with the experimental results presented here). Thus, results in Fig. 8 show that above 25% OOH, steric hindrance or modification of chain stacking certainly causes some of the –OOH groups to position themselves toward the interior of the bilayer (state 2 in Fig. 9).

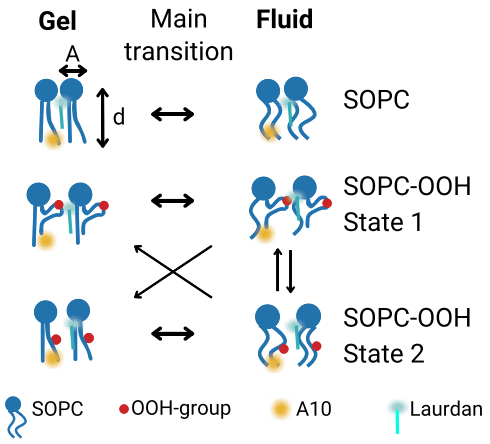

FIG. 9. Schematic illustration of the possible orientation of the hydroperoxide (–OOH) groups in hydroperoxidized SOPC membranes in gel and fluid phases. The –OOH group can be oriented toward the membrane surface, interacting with interfacial water molecules (state 1) or embedded within the bilayer (state 2). The position of the –OOH group may change upon phase transition, reflecting a two-stage transition process.

D. A possible scenario for thermal changes as a function of the bilayer composition

Previous theoretical work has noted the propensity of hydroperoxide groups to migrate toward the lipid–water interface. When present in low concentrations, –OOH groups are primarily found there with the other chain inserted among the SOPC acyl chains, a situation depicted as *State 1* in the schematic of Fig. 9. As the concentration of peroxides increases, competition for the area limited interface becomes fierce and a more standard *State 2* with both chains lying in the hydrophobic core (Fig. 9) becomes competitive, with a probability of occurrence on par with the exposed state 1.[18,19]

By analyzing sequences of lipids with similar chains but increasingly hydrophilic headgroups, it was established that the main transition temperature T_m decreases with the degree of hydrophilicity.[20] With two hydrophilic moieties and a single chain melting, the presence of state 1 SOPC-OOH is thus likely to drive both T_m and ΔH down to lower values.

State 2 SOPC-OOH reverses the trend regarding the jump in enthalpy, until reaching values as high as $\Delta H_{SOPCOOH}$ = 30 kJ/mol (fully peroxidized bilayer, states 1 and 2 combined). An enlargement or a duplication of the melting transition can be justified remembering that fully peroxidized bilayers are mixtures of 2 *trans* isomers (due to the dye sensitized peroxidation mechanism), as already shown in Fig. 1. The packed gel phase of state 2 SOPC-OOH is not well understood nor described yet, but seems to be more cohesive than its unsaturated counterpart. As a result, a large ΔH is seen, which could result from the combination of three factors: (i) a tight cohesive packing favored by the trans C=C bonds, (ii) attractive –OOH interactions leading to "transient dimer formation" deep into the hydrophobic layers, and (iii) a more disordered fluid state with higher concentration of gauche–gauche conformational isomers correlated with a thinner membrane and a larger area per lipid (as well as a smaller "deuterium S_{CD} order parameter"). The large change in enthalpy is paralleled by a corresponding large change in entropy.

We thus advocate the following possible mechanism: As its concentration increases from 0% to 25%, SOPC–OOH populates the bilayer as state 1 and T_m decreases sharply as would do a mixture of SOPC with a low melting point ($\leq -18\,^{\circ}$C), low ΔH lipid. Peroxidized lipids are somewhat acting as *impurities* reducing the strength of the melting transition.

At some point, the fraction of –OOH exposed at the interface saturates and does not increase further as x grows. In parallel, the Laurdan GP signal levels off, suggesting that the bilayer interfacial region has reached a stable state, which decouples from the melting processes occurring deeper into the hydrophobic region. In the 25%–100% concentration range, the melting temperature gently decreases to reach the value $T_m \simeq [-5, -3]\,^{\circ}$C of a fully peroxidized bilayer.

The structural changes upon heating of a fully peroxidized bilayer, therefore, seem to happen as two consecutive transitions. A first broad transition, reported by DSC and A10 fluorescence, is likely to be associated with a melting of the chains forming the

hydrophobic layer, from a strong cohesive to a highly disorganized and anisotropic state, accompanied by a strong calorimetric signal. A second transition affecting only the interfacial region is reported by Laurdan. This second transition, with no or little calorimetric signature, seems entropy driven, involving interfacial water molecules. One should bear in mind that a more complex interplay between the bilayer structural changes and probes conformations could be at work as well.[21]

V. CONCLUSION

The peculiar molecular organization described above provides an explanation for the asymmetric and two-component DSC transition for fully hydroperoxidized SOPC bilayers, as the repositioning of –OOH groups and the cooperative freezing of acyl chains may occur as partially distinct events. The schematic shown in Fig. 9 illustrates this concept: hydroperoxide groups can adopt either surface-exposed or partially buried orientations, and their redistribution upon cooling contributes to the complex, broadened transition behavior observed experimentally.

The quantitative picture of hydroperoxidation-induced membrane remodeling established here opens several avenues for future investigation. Phase transitions and bilayer structural parameters, thickness, polarity, and chain ordering are known to govern the activity and conformational stability of membrane-associated proteins, ion channels, and enzymes. The well-defined SOPC/SOPC–OOH system introduced here, with its experimentally accessible transition temperatures and tunable oxidation levels, provides a controlled platform for dissecting how oxidative lipid damage modulates such protein functions under conditions directly relevant to cellular oxidative stress. In particular, the sharp decrease in transition temperature and the progressive loss of membrane cooperativity observed at low oxidation levels suggest that even modest degrees of hydroperoxidation may be sufficient to alter the thermodynamic environment experienced by membrane proteins, with potential consequences for their folding, lateral organization, and activity. This system, therefore, offers a well-characterized starting point for studies of lipid–protein interactions under oxidative conditions, where the degree of membrane perturbation can be precisely controlled and quantified. The two-state distribution of –OOH groups identified here, surface-exposed at low oxidation levels, progressively populating the bilayer interior above roughly 25%, carries implications beyond the thermodynamic characterization presented. Bilayers in which a fraction of hydroperoxide groups reside in the hydrophobic core represent compositionally heterogeneous matrices with spatially distinct physicochemical environments. Such structural heterogeneity may influence lateral lipid organization and the potential formation of oxidation-enriched domains, with consequences for membrane permeability and the partitioning of membrane-active molecules. In the context of lipid-based drug delivery, these findings suggest that the permeability and structural integrity of lipid nanoparticles or liposomal carriers under oxidative conditions will depend sensitively on the spatial distribution of oxidized lipids within the bilayer, a parameter that the present framework now allows to be addressed in a controlled and quantitative manner. The existence of a compositional threshold near 25% –OOH, above which buried hydroperoxide groups become significant, may also be relevant to the design of oxidation-responsive delivery systems with tunable release properties. The agreement between this experimentally determined threshold and the molecular dynamics predictions reported for POPC bilayers by Junqueira and coworkers[19] is notable. Despite differences in synthesis route and chain composition, the critical concentration at which –OOH groups begin to populate the bilayer interior appears to be conserved between SOPC and POPC, two of the most abundant monounsaturated phospholipid species in mammalian membranes. This convergence suggests that the two-state –OOH distribution described here may be a general feature of monounsaturated hydroperoxidized phospholipids rather than a peculiarity of the SOPC system and that the thermodynamic and structural consequences characterized here may be broadly applicable to membrane peroxidation in pathological contexts, such as neurodegeneration, inflammation, and ischemia-reperfusion injury, where oxidized phospholipids accumulate in cell membranes at biologically relevant concentrations. Finally, the complementary use of A10 and Laurdan as spatially distinct fluorescent reporters proved instrumental in resolving the layered nature of the phase transition. Laurdan, anchored near the headgroup region, reported interfacial changes that saturated above 50% oxidation, while A10, embedded more deeply in the hydrophobic core, continued to track ordering changes across the full composition range and consistently reported lower transition temperatures. This spatial decoupling of the two probes provides a methodological contribution that extends beyond the specific system studied here. The combination of A10 and Laurdan as complementary bilayer reporters, one sensitive to the interfacial region and another to the hydrophobic interior, could be deployed more broadly to characterize the depth-resolved response of membranes to other chemical modifications, including truncated oxidation products, ether lipids, or cholesterol-depleted systems, as well as in more complex biomimetic or cellular environments where monitoring lipid peroxidation *in situ* remains technically challenging.

SUPPLEMENTARY MATERIAL

The supplementary material provides figures corresponding to the data acquired using the different techniques employed in this work.

ACKNOWLEDGMENTS

This work was supported by the Marie Skłodowska-Curie Doctoral Network ComeInCell, funded by the European Union's Horizon Europe research and innovation programme under the Grant Agreement No. 101168939. We thank A. Banyasz and O. Maury for help with the experimental setup, H. Hassani for help during data acquisition and M. Legros who headed the chemical characterization platform CARMAC of ICS.

AUTHOR DECLARATIONS

Conflict of Interest

The authors have no conflicts to disclose.

Author Contributions

E.L. and S.v.T. contributed equally to this work.

Eulalie Lafarge: Conceptualization (equal); Data curation (equal); Formal analysis (equal); Investigation (equal); Methodology (equal); Software (equal); Validation (equal); Visualization (lead); Writing – original draft (equal); Writing – review & editing (equal). **Sifre van Teeffelen**: Conceptualization (equal); Data curation (lead); Formal analysis (lead); Investigation (lead); Methodology (lead); Software (lead); Validation (equal); Visualization (equal); Writing – original draft (lead); Writing – review & editing (lead). **André P. Schroder**: Conceptualization (equal); Data curation (equal); Formal analysis (supporting); Investigation (equal); Methodology (supporting); Software (equal); Supervision (supporting); Validation (equal); Visualization (equal); Writing – original draft (equal); Writing – review & editing (equal). **Pierre Muller**: Conceptualization (supporting); Data curation (supporting); Investigation (supporting); Methodology (supporting); Software (supporting); Visualization (supporting); Writing – original draft (supporting); Writing – review & editing (supporting). **Fabrice Thalmann**: Conceptualization (supporting); Formal analysis (equal); Investigation (supporting); Validation (equal); Visualization (supporting); Writing – original draft (supporting); Writing – review & editing (supporting). **Yann Bretonnière**: Formal analysis (supporting); Investigation (supporting); Methodology (supporting); Writing – review & editing (supporting). **Lorenzo Metilli**: Data curation (supporting); Formal analysis (supporting); Investigation (supporting); Methodology (supporting); Writing – review & editing (supporting). **Apostolos Vagias**: Data curation (supporting); Formal analysis (supporting); Investigation (supporting); Visualization (supporting); Writing – review & editing (supporting). **Léo Corne**: Investigation (equal); Methodology (equal); Software (equal); Supervision (supporting); Writing – review & editing (supporting). **Carlos M. Marques**: Conceptualization (lead); Data curation (equal); Formal analysis (lead); Funding acquisition (equal); Investigation (equal); Methodology (equal); Project administration (lead); Resources (lead); Software (equal); Supervision (lead); Validation (equal); Visualization (equal); Writing – original draft (lead); Writing – review & editing (lead).

DATA AVAILABILITY

The data that support the findings of this study are openly available in Zenodo, at 10.5281/zenodo.18261256, reference number. Raw data were generated partly at Institut Laue Langevin. Derived data supporting the findings of this study are available from the corresponding author upon reasonable request.

REFERENCES

[1] B. Alberts, R. Heald, A. Johnson, D. Morgan, M. Raff, K. Roberts, and P. Walter, *Molecular Biology of the Cell: Seventh International Student Edition with Registration Card* (WW Norton & Company, 2022).

[2] O. G. Mouritsen, *Life as a Matter of Fat*, 1st ed. (Springer-Verlag, Berlin Heidelberg, 2005).

[3] T. Heimburg, "Membrane structure," in *Thermal Biophysics of Membranes* (Wiley-VCH Verlag GmbH & Co. KGaA, 2007).

[4] A. Ayala, M. F. Muñoz, and S. Argüelles, "Lipid peroxidation: Production, metabolism, and signaling mechanisms of malondialdehyde and 4-hydroxy-2-nonenal," Oxid. Med. Cell. Longevity **2014**(1), 360438.

[5] V. N. Bochkov, O. V. Oskolkova, K. G. Birukov, A.-L. Levonen, C. J. Binder, and J. Stöckl, "Generation and biological activities of oxidized phospholipids," Antioxid. Redox Signaling **12**(8), 1009–1059 (2010).

[6] M. Paez-Perez, A. Vyšniauskas, I. López-Duarte, E. J. Lafarge, R. López-Ríos De Castro, C. M. Marques, A. P. Schroder, P. Muller, C. D. Lorenz, N. J. Brooks, and M. K. Kuimova, "Directly imaging emergence of phase separation in peroxidized lipid membranes," Commun. Chem. **6**(1), 15 (2023).

[7] G. Wang, H.-n. Lin, S. Li, and C.-h. Huang, "Phosphatidylcholines with sn^{-1} saturated and sn^{-2} *cis*-monounsaturated acyl chains: Their melting behavior and structures," J. Biol. Chem. **270**(39), 22738–22746 (1995).

[8] A. S. Klymchenko and R. Kreder, "Fluorescent probes for lipid rafts: From model membranes to living cells," Chem. Biol. **21**(1), 97–113 (2014).

[9] T. Parasassi, G. De Stasio, A. d'Ubaldo, and E. Gratton, "Phase fluctuation in phospholipid membranes revealed by Laurdan fluorescence," Biophys. J. **57**(6), 1179–1186 (1990).

[10] Z. Zheng, F. Caraguel, Y.-Y. Liao, C. Andraud, B. van Der Sanden, and Y. Bretonnière, "Photostable far-red emitting pluronic silicate nanoparticles: Perfect blood pool fluorophores for biphotonic *in vivo* imaging of the leaky tumour vasculature," RSC Adv. **6**(96), 94200–94205 (2016).

[11] SAM instrument layout-ill neutrons for society, 2025, see https://www.ill.eu/for-all-users/instruments/instruments-list/sam/description/instrument-layout.

[12] C. D. Dewhurst, "Graphical reduction and analysis small-angle neutron scattering program: Grasp," J. Appl. Crystallogr. **56**(5), 1595–1609 (2023).

[13] D. M. Sadler and D. L. Worcester, "Neutron scattering studies of photosynthetic membranes in aqueous dispersion," J. Mol. Biol. **159**(3), 485–499 (1982).

[14] E. Lafarge, C. M. Marques, M. Schmutz, P. Muller, and A. P. Schroder, "Thickness determination of hydroperoxidized lipid bilayers from medium-resolution cryo-tem images," Methods Enzymol. **700**, 329–348 (2024).

[15] N. Watanabe, Y. Goto, K. Suga, T. K. M. Nyholm, J. P. Slotte, and H. Umakoshi, "Solvatochromic modeling of Laurdan for multiple polarity analysis of dihydrosphingomyelin bilayer," Biophys. J. **116**(5), 874–883 (2019).

[16] J. Wong-Ekkabut, Z. Xu, W. Triampo, I.-M. Tang, D. Peter Tieleman, and L. Monticelli, "Effect of lipid peroxidation on the properties of lipid bilayers: A molecular dynamics study," Biophys. J. **93**(12), 4225–4236 (2007).

[17] P. Boonnoy, V. Jarerattanachat, M. Karttunen, and J. Wong-Ekkabut, "Bilayer deformation, pores, and micellation induced by oxidized lipids," J. Phys. Chem. Lett. **6**(24), 4884–4888 (2015).

[18] L. Rems, M. Viano, M. A. Kasimova, D. Miklavčič, and M. Tarek, "The contribution of lipid peroxidation to membrane permeability in electropermeabilization: A molecular dynamics study," Bioelectrochemistry **125**, 46–57 (2019).

[19] H. Junqueira, A. P. Schroder, F. Thalmann, A. Klymchenko, Y. Mély, M. S. Baptista, and C. M. Marques, "Molecular organization in hydroperoxidized popc bilayers," Biochim. Biophys. Acta, Biomembr. **1863**(10), 183659 (2021).

[20] D. Marsh, "Structural and thermodynamic determinants of chain-melting transition temperatures for phospholipid and glycolipids membranes," Biochim. Biophys. Acta, Biomembr. **1798**, 40–51 (2010).

[21] A. Lester, H. Orlikowska-Rzeznik, E. Krok, and L. Piatkowski, "Laurdan adopts distinct, phase-specific orientations in lipid membranes," J. Phys. Chem. B **129**, 6233 (2025).

Supplementary Materials for: Main phase transition of hydroperoxidized SOPC bilayers

Eulalie Lafarge[1,1], Sifre van Teeffelen[1,1], André P. Schroder[1], Pierre Muller[1], Yann Bretonnière[1], Lorenzo Metilli[1], Apostolos Vagias[1], Léo Corne[1], Carlos M. Marques[1,]

[a]*Institut Charles Sadron, CNRS UPR22 & Université de Strasbourg, Strasbourg, 67000, France*
[b]*University of Lyon, ENS-Lyon, CNRS UMR 5182, Chem. Lab, Lyon, 69342, France*
[c]*CNRS, INSA Lyon,LaMCoS UMR5259, Villeurbanne, 69621, France*
[d]*Laboratoire Léon Brillouin, UMR12 CEA-CNRS, Gif-sur-Yvette, Grenoble, 91191, France*
[e]*ILL, Institut Laue-Langevin, 71 avenue des Martyrs, Grenoble, 38042, France*

1. Supplementary Figures

*corresponding author carlos.marques@ens-lyon.fr
[1]These authors contributed equally to the work

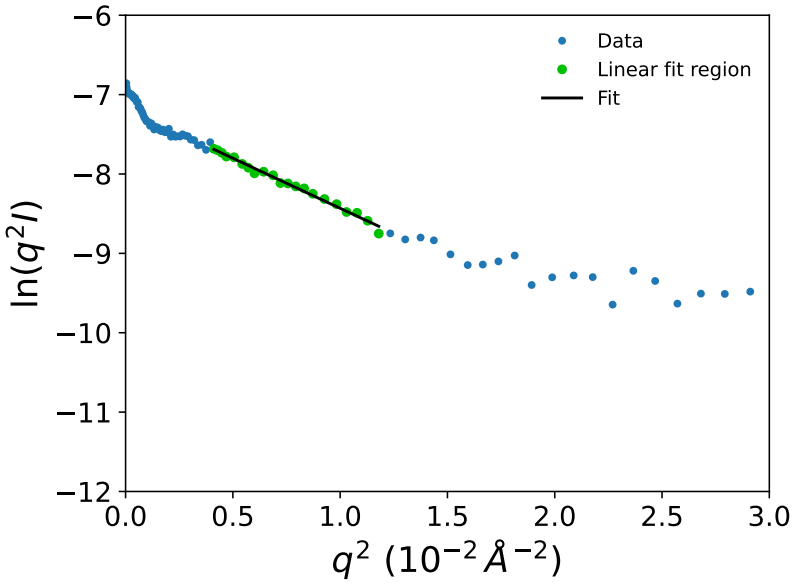

Figure S1: Plot of $\ln(q^2 I)$ as a function of q^2 for SOPC50/SOPCOOH50 at 4.6°C. The green points indicate the q^2-range (0.004-0.012) used for the linear regression, and the black line shows the resulting fit. The slope of this linear region is used to extract the membrane bilayer thickness.

Scatter plot showing ln of q squared times I on the y-axis (range approximately minus 12 to minus 6) as a function of q squared in units of 10 to the minus 2 inverse angstroms squared on the x-axis (range 0 to 3.0), for the SOPC 50 percent / SOPCOOH 50 percent sample at 4.6 degrees Celsius. The majority of data points are shown in blue and display a monotonically decreasing curve. A subset of points in the range q squared equal to 0.004 to 0.012 is highlighted in green, indicating the linear region used for the Guinier-type regression. A solid black line shows the linear fit through the green points. The slope of this linear region is used to extract the membrane bilayer radius of gyration and hence the bilayer thickness.

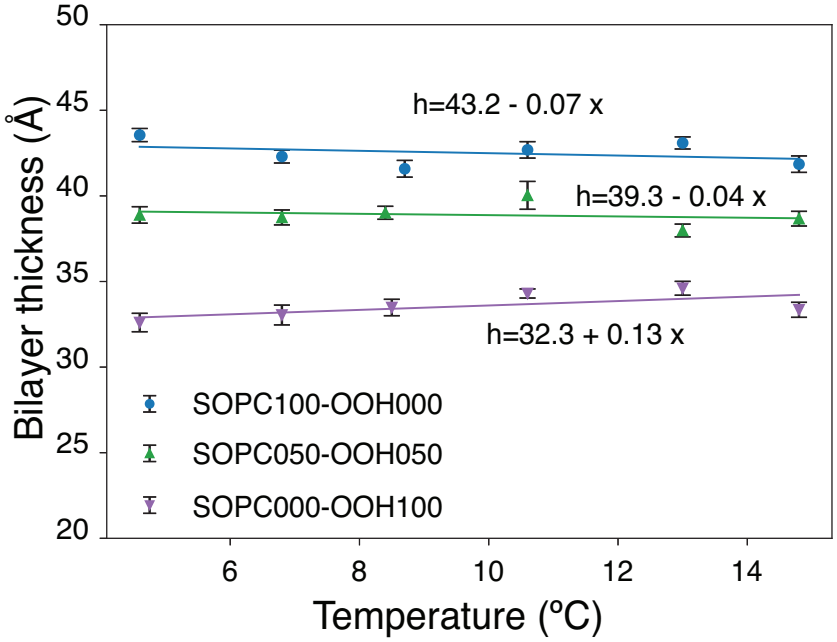

Figure S2: Bilayer thickness of SOPC, SOPC50/SOPCOOH50, and SOPCOOH liposomes as a function of temperature (T). Data points with vertical error bars represent the thickness extracted from the linear region of $\ln(q^2 I)$ vs q^2 for each SANS measurement, including the propagated uncertainty from the linear fit. Solid lines indicate linear fits to the thickness vs temperature (T) data for each sample.

Line plot showing bilayer thickness in angstroms on the y-axis (range 20 to 50) as a function of temperature in degrees Celsius on the x-axis (range 6 to 14) for three liposome compositions: pure SOPC (SOPC100-OOH000, blue squares), a 50:50 mixture (SOPC050-OOH050, green triangles), and fully hydroperoxidized SOPC (SOPC000-OOH100, purple inverted triangles). Each data point has a vertical error bar representing propagated uncertainty from the linear fit. Three solid lines show linear fits to the thickness versus temperature data for each sample. The fitted equations are h equals 43.2 minus 0.07 times T for pure SOPC, h equals 39.3 minus 0.04 times T for the 50:50 mixture, and h equals 32.3 plus 0.13 times T for fully hydroperoxidized SOPC. The bilayer thickness is nearly independent of temperature for all three compositions over the range explored, and the three datasets are vertically separated, with pure SOPC having the greatest thickness and fully hydroperoxidized SOPC the least.

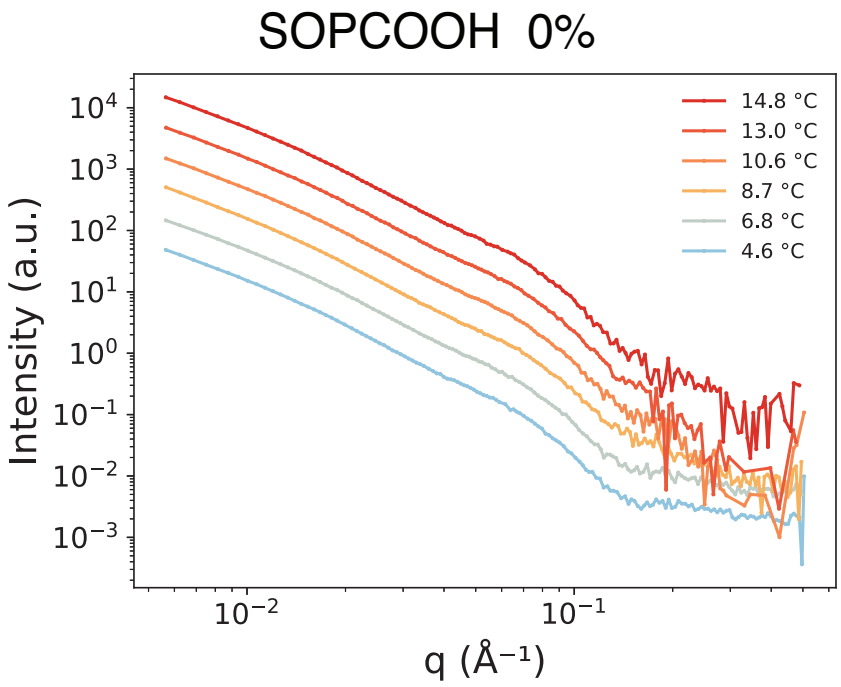

Figure S3: SANS intensity of SOPC liposomes at temperatures (T) of 4.6, 6.8, 8.7, 10.6, 13.0 and 14.8 °C. Curves are vertically offset for clarity.

Log-log plot showing SANS intensity in arbitrary units on the y-axis (range 10 to the minus 3 to 10 to the 4) as a function of scattering vector q in inverse angstroms on the x-axis (range approximately 10 to the minus 2 to 10 to the minus 1) for pure SOPC liposomes (SOPCOOH 0 percent) measured at six temperatures: 4.6, 6.8, 8.7, 10.6, 13.0, and 14.8 degrees Celsius. Each temperature is represented by a distinct color ranging from light blue at 4.6 degrees to dark red at 14.8 degrees. The curves are vertically offset for clarity and all show a monotonically decreasing power-law-like decay with increasing q, with no sharp features or peaks visible. The curves at higher temperatures are positioned above those at lower temperatures due to the vertical offset.

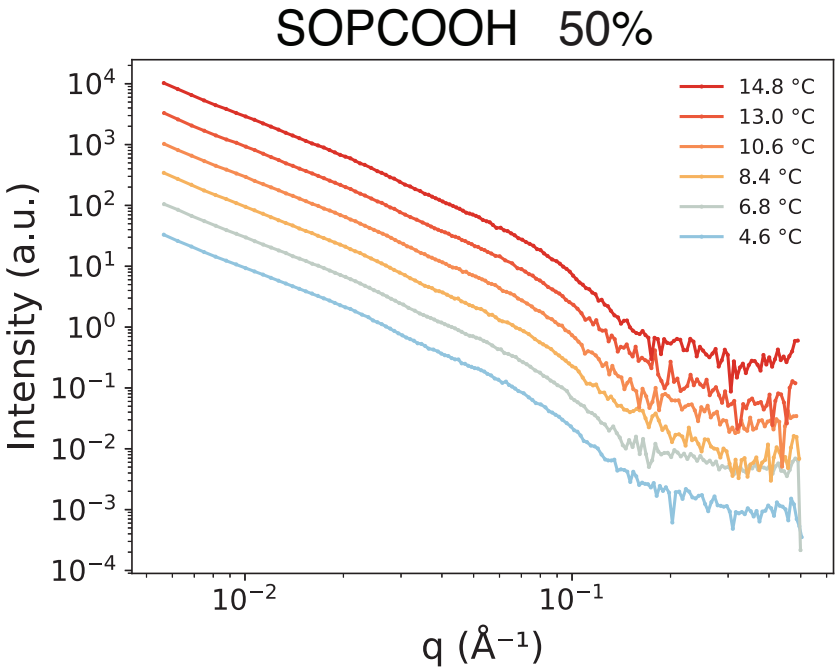

Figure S4: SANS intensity of liposomes with SOPC/SOPCOOH mixtures with 50% SOPCOOH at temperatures (T) of 4.6, 6.8, 8.4, 10.6, 13.0 and 14.8 °C. Curves are vertically offset for clarity.

Log-log plot showing SANS intensity in arbitrary units on the y-axis (range 10 to the minus 4 to 10 to the 4) as a function of scattering vector q in inverse angstroms on the x-axis (range approximately 10 to the minus 2 to 10 to the minus 1) for SOPC/SOPCOOH liposomes with 50 percent SOPCOOH measured at six temperatures: 4.6, 6.8, 8.4, 10.6, 13.0, and 14.8 degrees Celsius. Colors range from light blue at 4.6 degrees to dark red at 14.8 degrees. Curves are vertically offset for clarity and show a monotonically decreasing profile with increasing q. Compared to the pure SOPC sample, the curves display increased noise at high q values, particularly for lower temperatures, visible as irregular fluctuations in the curves at q values above approximately 0.05 inverse angstroms.

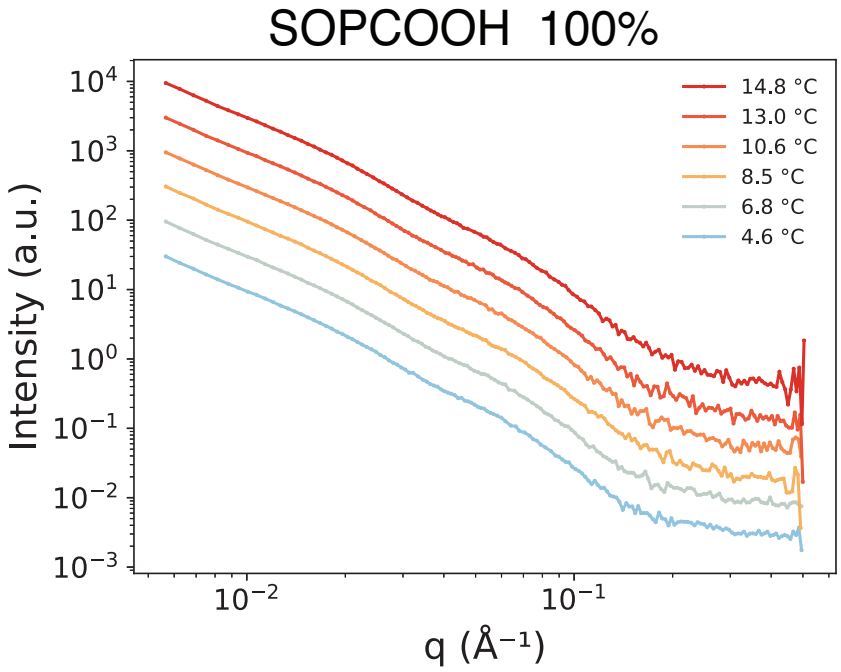

Figure S5: SANS intensity of fully hydroperoxidized SOPC liposomes at temperatures (T) of 4.6, 6.8, 8.5, 10.6, 13.0 and 14.8 °C. Curves are vertically offset for clarity.

Log-log plot showing SANS intensity in arbitrary units on the y-axis (range 10 to the minus 3 to 10 to the 4) as a function of scattering vector q in inverse angstroms on the x-axis (range approximately 10 to the minus 2 to 10 to the minus 1) for fully hydroperoxidized SOPC liposomes (SOPCOOH 100 percent) measured at six temperatures: 4.6, 6.8, 8.5, 10.6, 13.0, and 14.8 degrees Celsius. Colors range from light blue at 4.6 degrees to dark red at 14.8 degrees. Curves are vertically offset for clarity. The overall shape is qualitatively similar to the 0 percent and 50 percent samples, showing a monotonically decreasing power-law decay. The separation between curves at different temperatures appears more uniform compared to the other compositions.

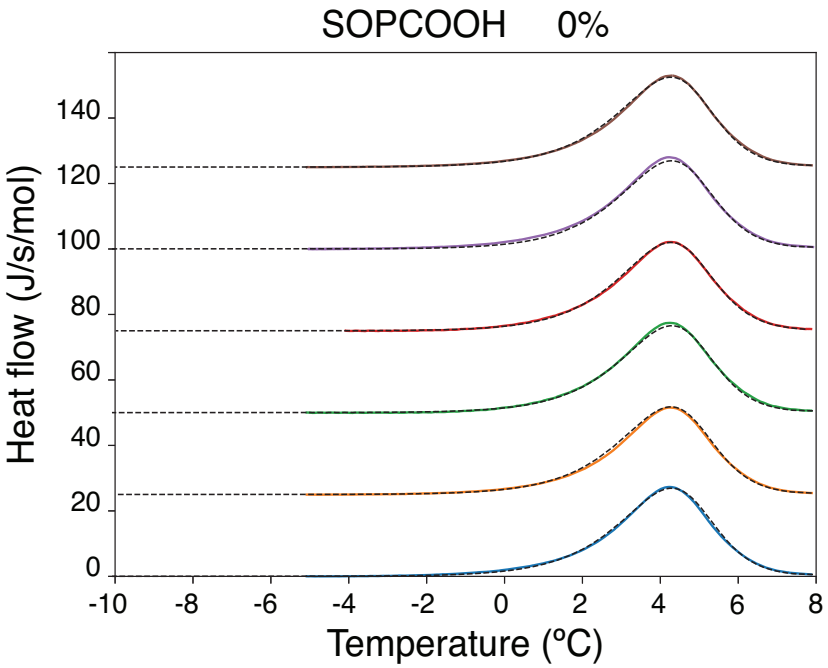

Figure S6: DSC traces of 3.32, 3.32, 3.27, 3.27, 3.25, 3.25 μmol SOPC (bottom to top), baseline subtracted, recorded during cooling at 0.25°C/min. ΔH = 21.3, 20.4, 21.0, 20.9, 22.2, 22.0 kJ/mol. Fits in dashed lines – see main text – provide $(T_{\mathrm{m}}, \Delta T)$ pairs in °C (5.05, 0.58), (5.06, 0.58), (5.02, 0.60), (5.05, 0.59), (5.06, 0.58), (5.07, 0.59). Cooperativity n = 51.

Stacked DSC thermograms for pure SOPC (SOPCOOH 0 percent) showing heat flow in joules per second per mole on the y-axis (range 0 to 140) as a function of temperature in degrees Celsius on the x-axis (range minus 10 to plus 8). Six replicate cooling scans at 0.25 degrees Celsius per minute are shown stacked vertically, each in a different color, with baselines offset proportionally for clarity. Each trace shows a sharp, symmetric, bell-shaped peak centered near 5 degrees Celsius, characteristic of a cooperative main phase transition. Dashed lines overlay each trace showing the single-component transition function fit. The peak shape and position are highly reproducible across replicates. The transition enthalpy values range from 20.4 to 22.2 kilojoules per mole and transition temperatures fall between 5.02 and 5.07 degrees Celsius with transition widths near 0.59 degrees Celsius. The cooperativity index n is 51.

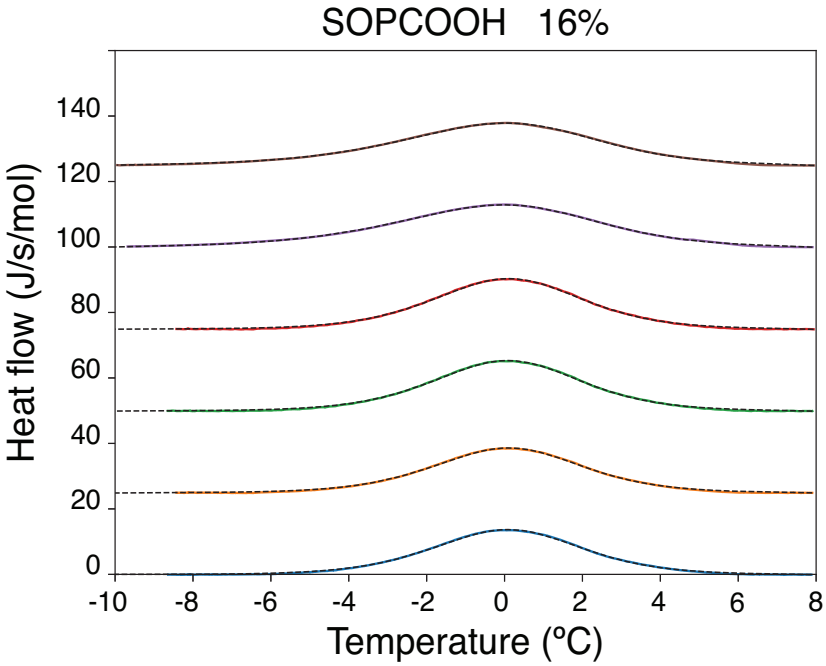

Figure S7: DSC traces of 2.70, 2.70, 3.01, 3.01, 3.82, 3.82 μmol SOPC/SOPCOOH mixtures with 16% SOPCOOH (bottom to top), baseline subtracted. ΔH = 16.2, 16.1, 18.0, 18.1, 20.8, 20.1 kJ/mol. Fits in dashed lines – see main text – provide $(T_{\mathrm{m}}, \Delta T)$ pairs (0.57, 1.21), (0.59 ,1.21), (0.56, 1.21), (0.6, 1.21), (1.17, 1.44), (1.19, 1.41). Cooperativity n = 27.

Stacked DSC thermograms for SOPC/SOPCOOH mixtures with 16 percent SOPCOOH showing heat flow in joules per second per mole on the y-axis (range 0 to 140) as a function of temperature in degrees Celsius on the x-axis (range minus 10 to plus 8). Six replicate cooling scans are shown stacked and offset for clarity, each in a different color. Compared to pure SOPC, the transition peaks are shifted to lower temperatures near 0 to 1 degree Celsius, are broader and lower in amplitude, and show a slight asymmetry. Dashed fit lines overlay each trace. Transition enthalpies range from 16.1 to 20.8 kilojoules per mole, transition temperatures fall between 0.56 and 1.19 degrees Celsius, and transition widths are approximately 1.21 to 1.44 degrees Celsius. The cooperativity index n is 27.

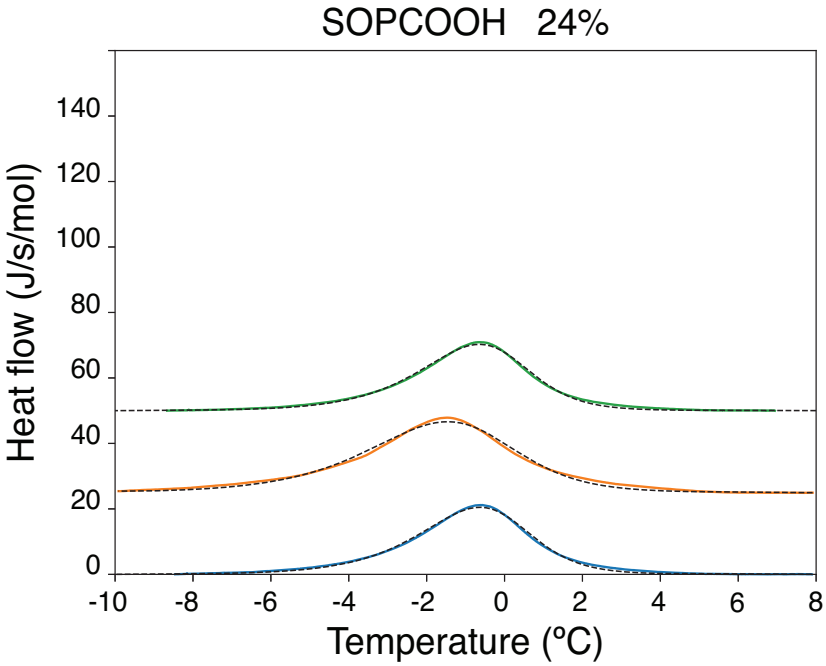

Figure S8: DSC traces of 3.15, 4.37, 3.15 μmol SOPC/SOPCOOH mixtures with 24% SOPCOOH (bottom to top), baseline subtracted. ΔH = 19.2, 26.7, 18.8 kJ/mol. Fits in dashed lines – see main text – provide $(T_{\mathrm{m}}, \Delta T)$ pairs (0.17, 0.73), (-0.44, 1.0), (0.2,0.73). Cooperativity n = 38.

Stacked DSC thermograms for SOPC/SOPCOOH mixtures with 24 percent SOPCOOH showing heat flow in joules per second per mole on the y-axis (range 0 to 140) as a function of temperature in degrees Celsius on the x-axis (range minus 10 to plus 8). Three replicate cooling scans are shown stacked and offset for clarity, in blue, orange, and green. The transition peaks are shifted further to lower temperatures compared to 16 percent SOPCOOH, centered near minus 0.2 to plus 0.2 degrees Celsius, and are somewhat broader. Dashed fit lines overlay each trace. Transition enthalpies are 18.8, 19.2, and 26.7 kilojoules per mole; transition temperatures range from minus 0.44 to plus 0.20 degrees Celsius with transition widths of 0.73 to 1.0 degrees Celsius. The cooperativity index n is 38.

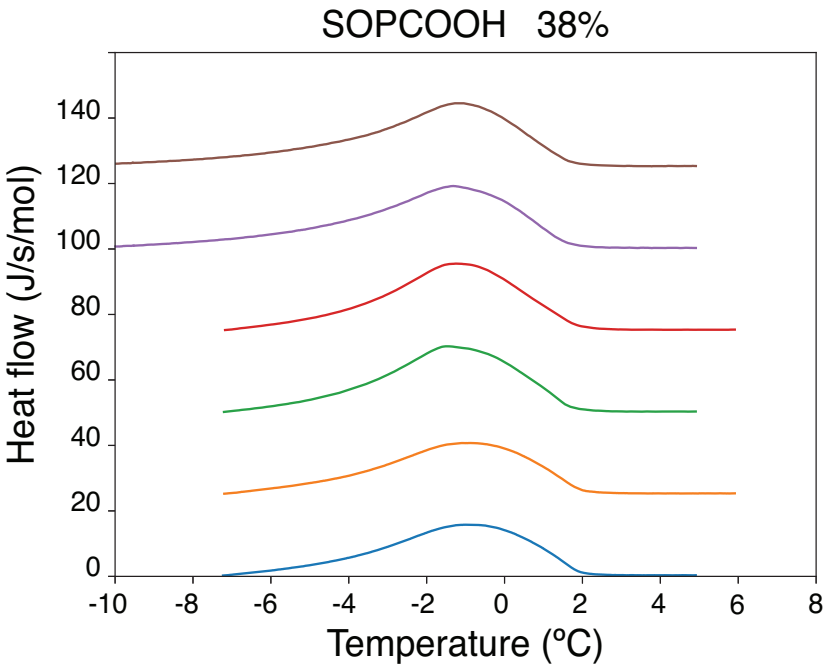

Figure S9: DSC traces of 3.97, 3.97, 7.95, 7.95, 4.0, 4.0 μmol SOPC/SOPCOOH mixtures with 38% SOPCOOH (bottom to top), baseline subtracted. ΔH = 16.8, 16.9, 20.0, 20.0, 22.1, 22.3 kJ/mol. Traces indicate coexistence of two phases, precluding a fit with one or two transition processes.

Stacked DSC thermograms for SOPC/SOPCOOH mixtures with 38 percent SOPCOOH showing heat flow in joules per second per mole on the y-axis (range 0 to 140) as a function of temperature in degrees Celsius on the x-axis (range minus 10 to plus 8). Six replicate cooling scans are shown stacked and offset, each in a different color. The transition peaks are centered near minus 2 degrees Celsius and are markedly broader and more asymmetric than at lower oxidation levels, with a broad shoulder or secondary feature visible. No dashed fit lines are shown, as the traces indicate coexistence of two phases that precludes fitting with one or two simple transition functions. Transition enthalpies range from 16.8 to 22.3 kilojoules per mole.

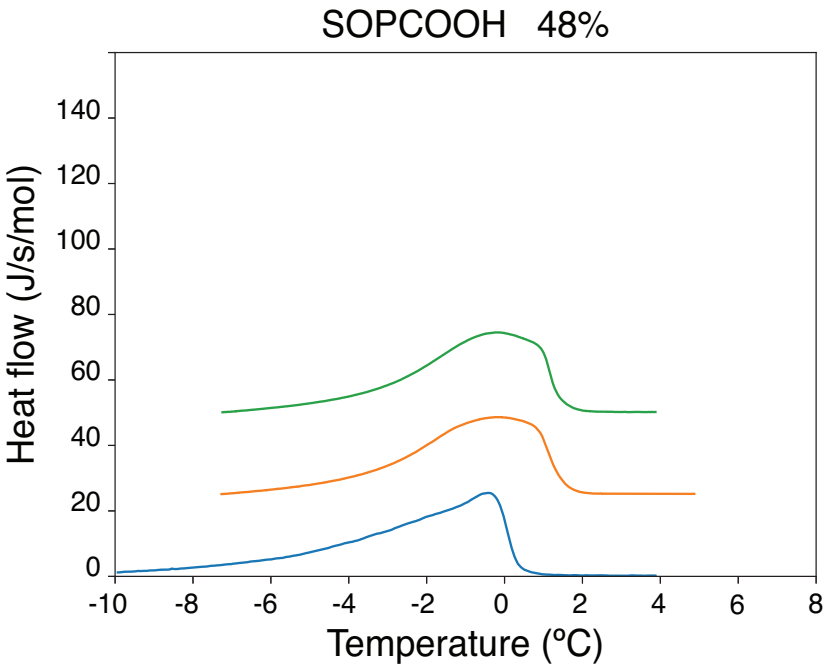

Figure S10: DSC traces of 3.56, 2.68, 2.68 μmol SOPC/SOPCOOH mixtures with 48% SOPCOOH (bottom to top), baseline subtracted. ΔH = 24.4, 22.4, 22,3 kJ/mol. Traces indicate coexistence of two phase, precluding a fit with one or two transition processes.

Stacked DSC thermograms for SOPC/SOPCOOH mixtures with 48 percent SOPCOOH showing heat flow in joules per second per mole on the y-axis (range 0 to 140) as a function of temperature in degrees Celsius on the x-axis (range minus 10 to plus 8). Three replicate cooling scans are shown stacked and offset in blue, orange, and green. The peaks are centered near minus 1 to 0 degrees Celsius and display a pronounced asymmetry with a sharp low-temperature onset and a broader high-temperature tail, indicative of coexistence of two phases. No fit lines are shown. Transition enthalpies are 22.3, 22.4, and 24.4 kilojoules per mole.

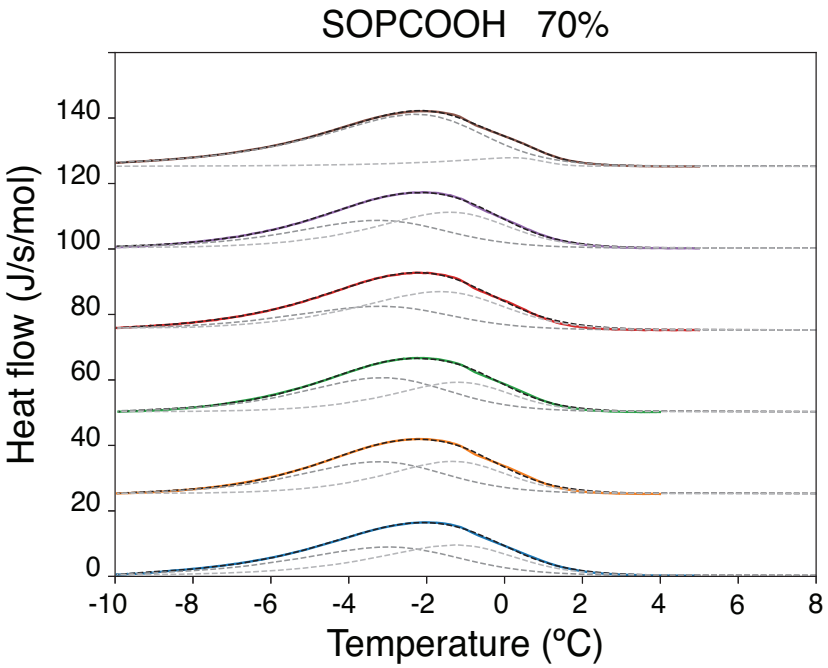

Figure S11: DSC traces of 3.38, 2.92, 2.92, 3.11, 3.11, 3.38 μmol SOPC/SOPCOOH mixtures with 70% SOPCOOH (bottom to top), baseline subtracted. ΔH = 22.3, 21.4, 21.2, 23.7, 22.7, 24.1 kJ/mol. Fits in dashed lines with two transition processes – see main text – provide $(T^1_{\mathrm{m}}, \Delta^1 T)$ and $(T^2_{\mathrm{m}}, \Delta^2 T)$ pairs [(-2.28, 1.02),(-0.47, 0.79)], [(-2.28, 1.02),(-0.47, 0.79)], [(-2.17, 1.39),(-0.32, 0.71)], [(-2.02, 1.03),(-0.54, 0.91)], [(-2.18, 1.03),(-0.42, 0.83)], [(-0.97, 0.93),(0.93, 0.3)].Cooperativity $n^1 = 44$ and $n^2 = 98$. Heat decomposition as $\Delta H = \Delta H_1 + \Delta H_2$ gives $f_H = \Delta H_1/\Delta H$ values f_H=0.54, 0.54, 0.58, 0.40, 0.47, 0.91.

Stacked DSC thermograms for SOPC/SOPCOOH mixtures with 70 percent SOPCOOH showing heat flow in joules per second per mole on the y-axis (range 0 to 140) as a function of temperature in degrees Celsius on the x-axis (range minus 10 to plus 8). Six replicate cooling scans are shown stacked and offset, each in a different color. Each trace shows a broad, asymmetric profile that can be deconvoluted into two overlapping components, shown as dashed lines for each transition. The two component peaks are centered near minus 2.2 and minus 0.4 degrees Celsius respectively for most replicates. Transition enthalpies range from 21.2 to 24.1 kilojoules per mole. The cooperativity indices are n1 equal to 44 and n2 equal to 98 for the two components. The fractional enthalpy contribution of the first component fH ranges from 0.40 to 0.91 across replicates.

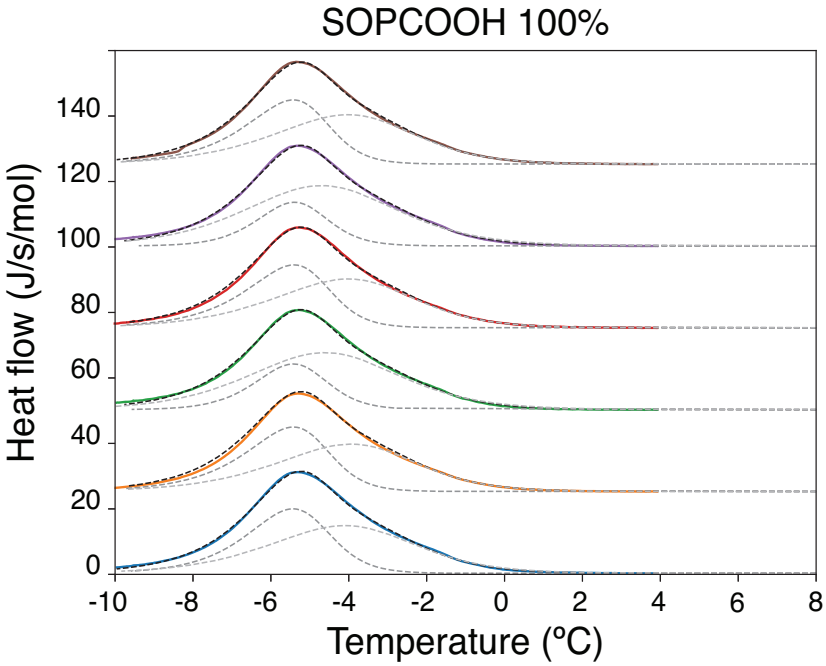

Figure S12: DSC traces of 3.33, 3.40, 3.30, 3.38, 3.38, 3.33 μmol of fully hydroperoxidized SOPC (bottom to top), baseline subtracted. ΔH = 31.4, 29.3, 30.9, 30.2, 31.3, 30.9 kJ/mol. Fits in dashed lines with two transition processes – see main text – provide $(T^1_{\rm m}, \Delta^1 T)$ and $(T^2_{\rm m}, \Delta^2 T)$ pairs [(-4.7, 0.54),(-3.2, 1.1)], [(-4.7, 0.5),(-3.02, 1.0)], [(-4.93, 0.52),(-4.0, 1.22)], [(-4.69, 0.49),(-3.09, 1.0)], [(-4.7, 0.53),(-4.2, 1.25)], [(-4.7, 0.49),(-3.1, 1.01)]. Cooperativity $n^1 = 99$ and $n^2 = 29$. Heat decomposition as $\Delta H = \Delta H_1 + \Delta H_2$ gives $f_H = \Delta H_1/\Delta H$ values f_H=0.44, 0.46, 0.28, 0.44, 0.25, 0.44.

Stacked DSC thermograms for fully hydroperoxidized SOPC liposomes (SOPCOOH 100 percent) showing heat flow in joules per second per mole on the y-axis (range 0 to 140) as a function of temperature in degrees Celsius on the x-axis (range minus 10 to plus 8). Six replicate cooling scans are shown stacked and offset, each in a different color. Each trace shows a broad, distinctly asymmetric profile with a sharp, narrow high-amplitude component superimposed on a broader lower-amplitude component, both visible as dashed fit lines. The two component peaks are centered near minus 4.7 and minus 3.1 to minus 4.2 degrees Celsius. Transition enthalpies range from 29.3 to 31.4 kilojoules per mole. The cooperativity indices are n1 equal to 99 and n2 equal to 29. The fractional enthalpy contribution of the first component fH ranges from 0.25 to 0.46.

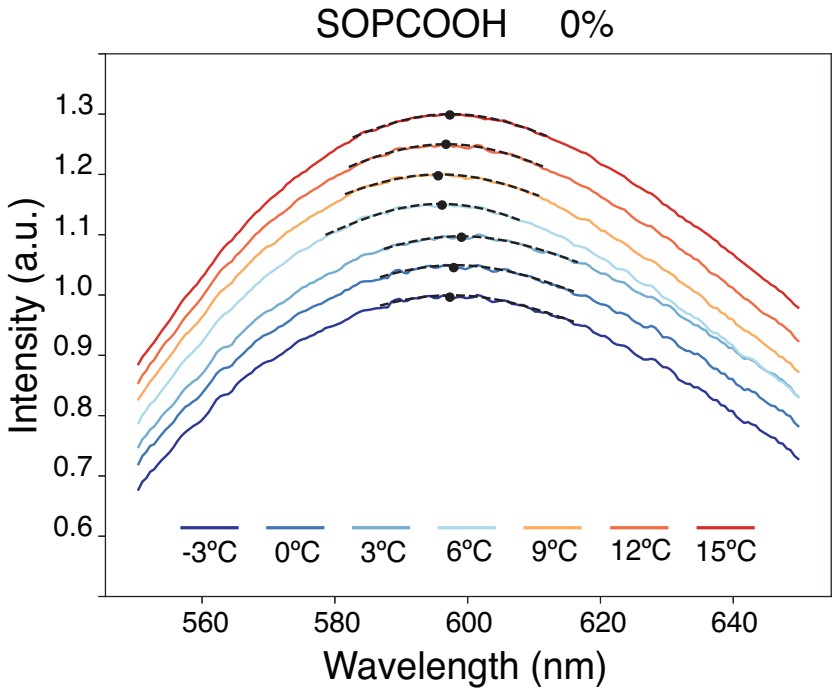

Figure S13: A10 emission spectra when inserted in SOPC liposomes at temperatures (T) of -3, 0, 3, 6, 9, 12 and 15 °C.

Line plot showing A10 fluorescence emission intensity in arbitrary units on the y-axis (range 0.6 to 1.3) as a function of emission wavelength in nanometres on the x-axis (range 560 to 640) for the probe inserted in pure SOPC liposomes (SOPCOOH 0 percent) at seven temperatures: minus 3, 0, 3, 6, 9, 12, and 15 degrees Celsius. Each temperature is represented by a distinct color, ranging from dark blue at minus 3 degrees to dark red at 15 degrees, as shown in the legend. All spectra show a broad, single-peaked emission band with a maximum near 600 nanometres. A filled black circle marks the position of the emission maximum on each curve. The peak intensity increases and the peak position shifts slightly to shorter wavelengths as temperature decreases, with the most pronounced shift occurring between 6 and 3 degrees Celsius, corresponding to the main phase transition of pure SOPC.

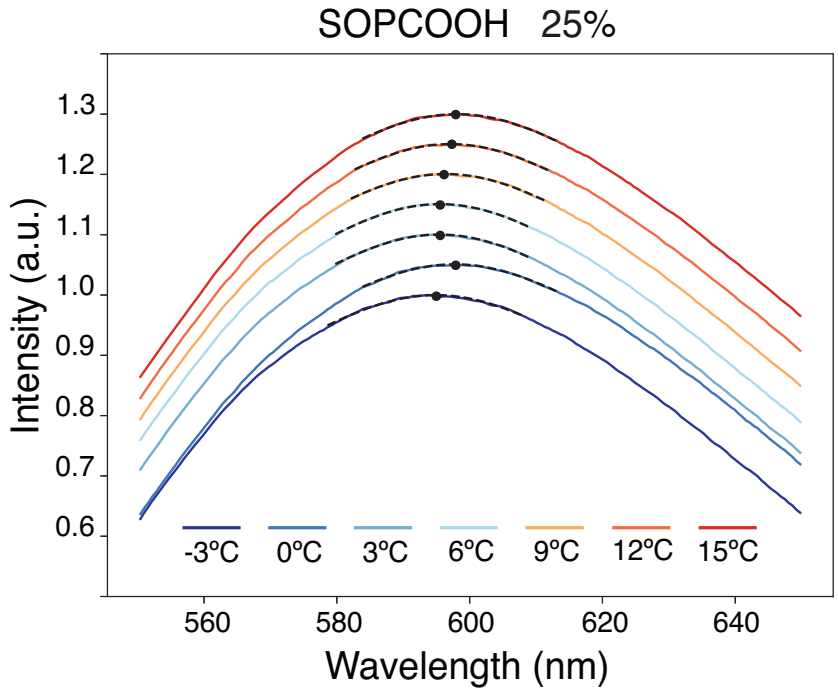

Figure S14: A10 emission spectra when inserted in SOPC/SOPCOOH mixtures with 25% SOPCOOH at temperatures (T) of -3, 0, 3, 6, 9, 12 and 15 °C.

Line plot showing A10 fluorescence emission intensity in arbitrary units on the y-axis (range 0.6 to 1.3) as a function of emission wavelength in nanometres on the x-axis (range 560 to 640) for the probe inserted in SOPC/SOPCOOH mixtures with 25 percent SOPCOOH at seven temperatures: minus 3, 0, 3, 6, 9, 12, and 15 degrees Celsius. Colors range from dark blue at minus 3 degrees to dark red at 15 degrees. All spectra show a broad single-peaked emission band near 600 nanometres. A filled black circle marks the emission maximum on each curve. Compared to pure SOPC, the spectral separation between curves at different temperatures is reduced, and the temperature-dependent blueshift of the peak maximum occurs at a lower temperature near 0 to 3 degrees Celsius, reflecting the downward shift of the phase transition temperature.

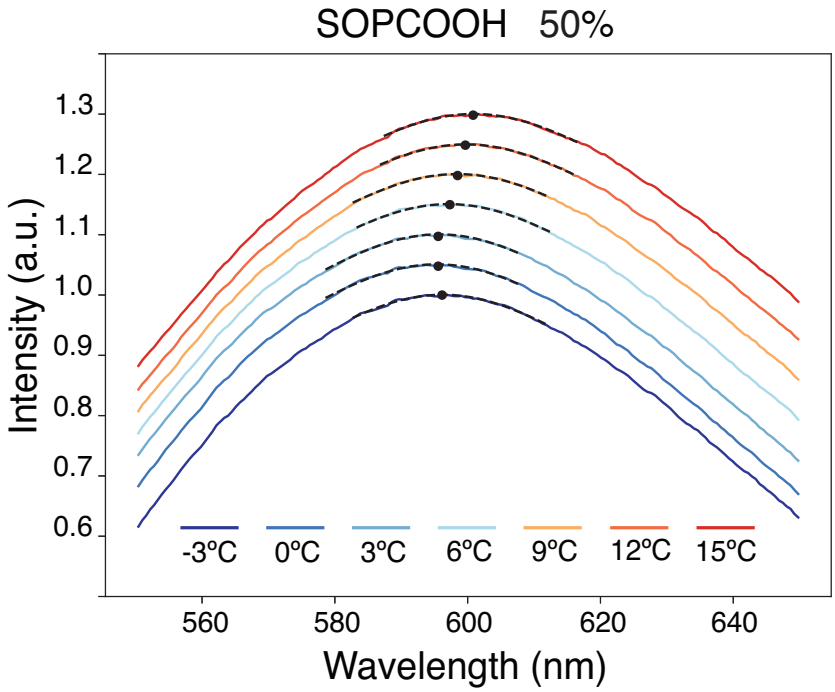

Figure S15: A10 emission spectra when inserted in SOPC/SOPCOOH mixtures with 50% SOPCOOH at temperatures (T) of -3, 0, 3, 6, 9, 12 and 15 °C.

Line plot showing A10 fluorescence emission intensity in arbitrary units on the y-axis (range 0.6 to 1.3) as a function of emission wavelength in nanometres on the x-axis (range 560 to 640) for the probe inserted in SOPC/SOPCOOH mixtures with 50 percent SOPCOOH at seven temperatures: minus 3, 0, 3, 6, 9, 12, and 15 degrees Celsius. Colors range from dark blue at minus 3 degrees to dark red at 15 degrees. All spectra show a broad single-peaked emission band near 600 nanometres. A filled black circle marks the emission maximum on each curve. The spectral spread between curves is further reduced compared to the 25 percent sample, and the transition-associated blueshift is centered near 0 degrees Celsius. The overall emission maximum position is shifted to slightly longer wavelengths compared to lower oxidation levels.

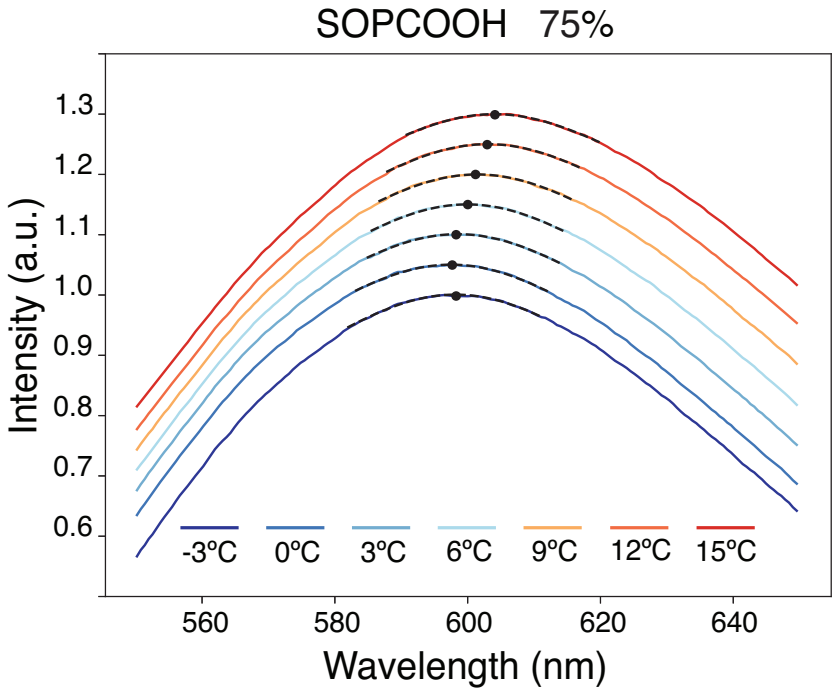

Figure S16: A10 emission spectra when inserted in SOPC/SOPCOOH mixtures with 75% SOPCOOH at temperatures (T) of -3, 0, 3, 6, 9, 12 and 15 °C.

Line plot showing A10 fluorescence emission intensity in arbitrary units on the y-axis (range 0.6 to 1.3) as a function of emission wavelength in nanometres on the x-axis (range 560 to 640) for the probe inserted in SOPC/SOPCOOH mixtures with 75 percent SOPCOOH at seven temperatures: minus 3, 0, 3, 6, 9, 12, and 15 degrees Celsius. Colors range from dark blue at minus 3 degrees to dark red at 15 degrees. All spectra show a broad single-peaked emission band. A filled black circle marks the emission maximum on each curve. The transition-associated blueshift is less pronounced and occurs at a lower temperature compared to lower oxidation levels. The emission maxima at all temperatures are shifted to longer wavelengths compared to less oxidized samples, reflecting increased bilayer polarity.

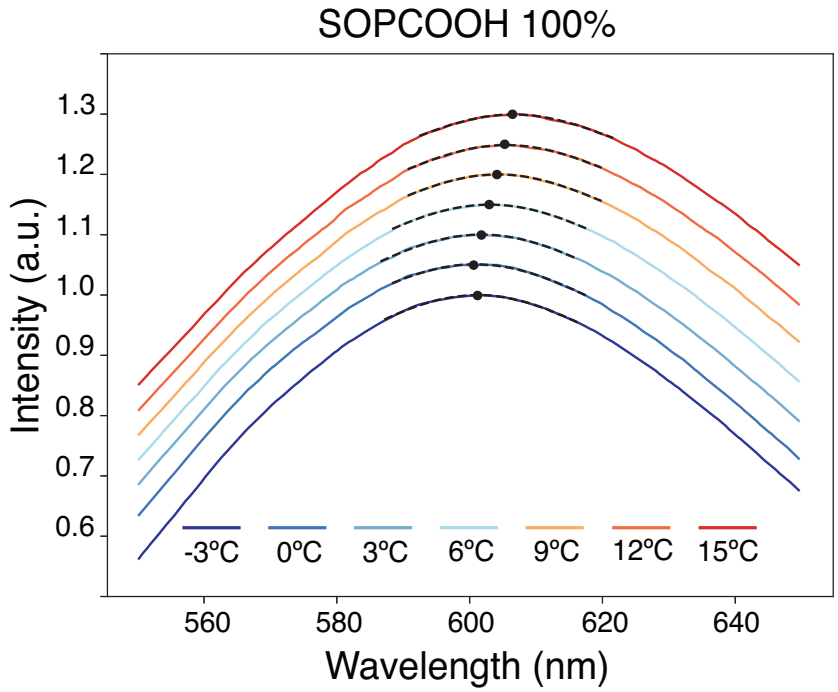

Figure S17: A10 emission spectra when inserted in full oxidized SOPC liposomes at temperatures (T) of -3, 0, 3, 6, 9, 12 and 15 °C.

Line plot showing A10 fluorescence emission intensity in arbitrary units on the y-axis (range 0.6 to 1.3) as a function of emission wavelength in nanometres on the x-axis (range 560 to 640) for the probe inserted in fully hydroperoxidized SOPC liposomes (SOPCOOH 100 percent) at seven temperatures: minus 3, 0, 3, 6, 9, 12, and 15 degrees Celsius. Colors range from dark blue at minus 3 degrees to dark red at 15 degrees. All spectra show a broad single-peaked emission band. A filled black circle marks the emission maximum on each curve. The spectral separation between temperatures is more uniform across the range compared to less oxidized samples, and the emission maxima are at the longest wavelengths observed across all compositions, consistent with a highly polar bilayer interior. The transition-associated blueshift is barely discernible and occurs near minus 3 to 0 degrees Celsius.

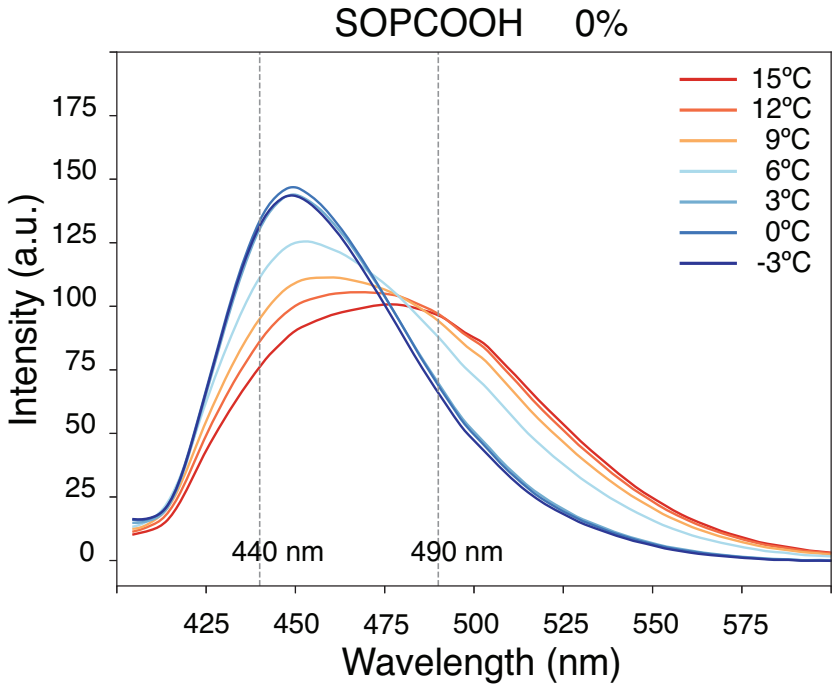

Figure S18: Laurdan emission spectra when inserted in SOPC liposomes at temperatures (T) of -3, 0, 3, 6, 9, 12 and 15 °C.

Line plot showing Laurdan fluorescence emission intensity in arbitrary units on the y-axis (range 0 to 175) as a function of emission wavelength in nanometres on the x-axis (range 425 to 575) for pure SOPC liposomes (SOPCOOH 0 percent) at seven temperatures: minus 3, 0, 3, 6, 9, 12, and 15 degrees Celsius. Colors range from dark blue at minus 3 degrees to dark red at 15 degrees, as shown in the legend. Two vertical dashed lines mark the wavelengths 440 and 490 nanometres used to calculate the generalized polarization. At minus 3 degrees Celsius (dark blue, gel phase), the spectrum shows a dominant emission peak near 440 nanometres and a smaller shoulder near 490 nanometres, indicating predominantly ordered lipid packing. At 15 degrees Celsius (dark red, fluid phase), the intensity at 440 nanometres decreases markedly and the emission near 490 nanometres increases, producing a broader, red-shifted spectrum. Intermediate temperatures show a progressive transition between these two spectral forms.

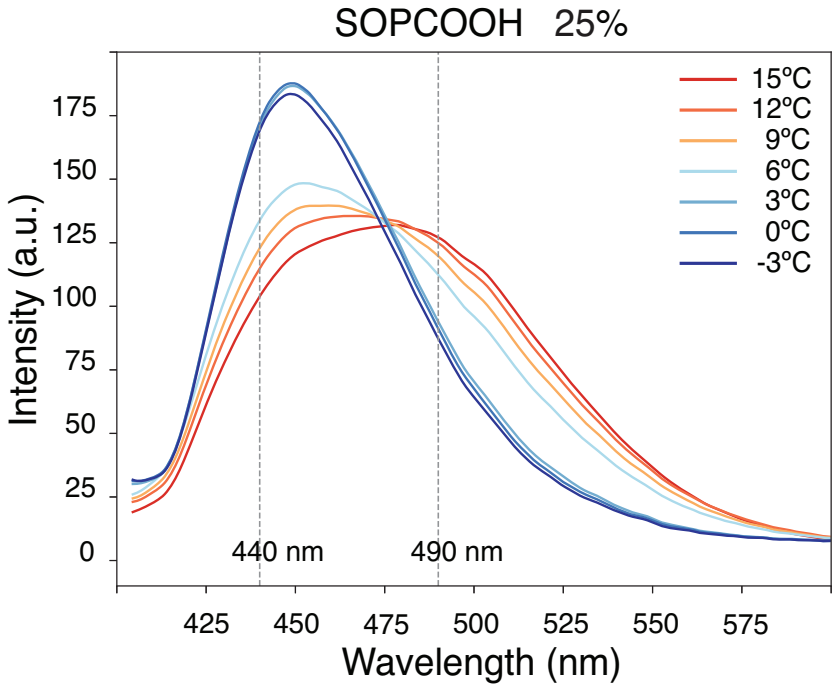

Figure S19: Laurdan emission spectra when inserted in SOPC/SOPCOOH mixtures with 25% SOPCOOH at temperatures (T) of -3, 0, 3, 6, 9, 12 and 15 °C.

Line plot showing Laurdan fluorescence emission intensity in arbitrary units on the y-axis (range 0 to 175) as a function of emission wavelength in nanometres on the x-axis (range 425 to 575) for SOPC/SOPCOOH mixtures with 25 percent SOPCOOH at seven temperatures: minus 3, 0, 3, 6, 9, 12, and 15 degrees Celsius. Colors range from dark blue at minus 3 degrees to dark red at 15 degrees. Two vertical dashed lines mark 440 and 490 nanometres. Compared to pure SOPC, the gel-phase spectrum (dark blue) shows a reduced peak at 440 nanometres and increased intensity at 490 nanometres relative to the pure SOPC gel-phase spectrum, indicating less ordered packing even in the gel state. The progressive temperature-dependent shift from 440-dominant to 490-dominant emission is preserved but the crossover between gel-like and fluid-like spectra occurs at a lower temperature.

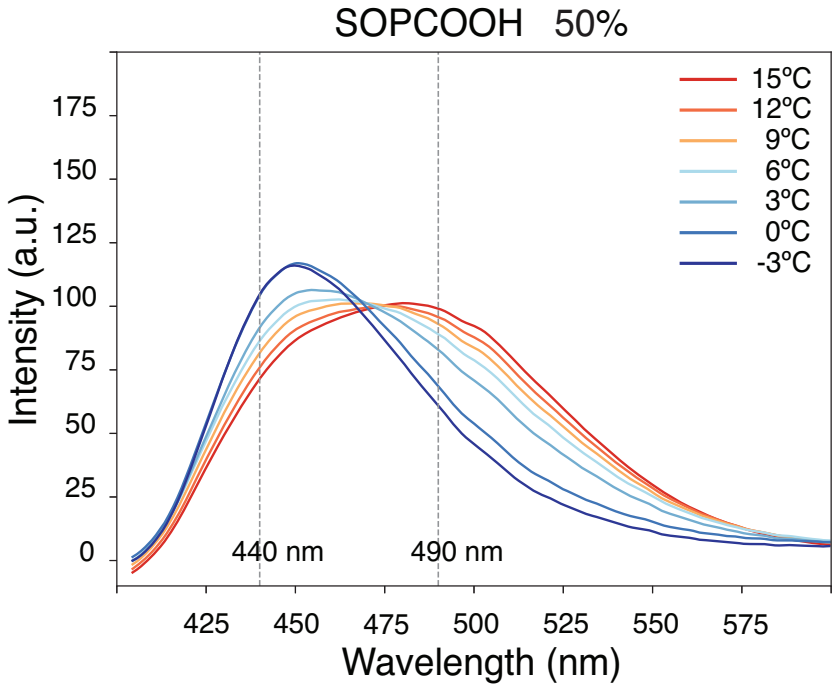

Figure S20: Laurdan emission spectra when inserted in SOPC/SOPCOOH mixtures with 50% SOPCOOH at temperatures (T) of -3, 0, 3, 6, 9, 12 and 15 °C.

Line plot showing Laurdan fluorescence emission intensity in arbitrary units on the y-axis (range 0 to 175) as a function of emission wavelength in nanometres on the x-axis (range 425 to 575) for SOPC/SOPCOOH mixtures with 50 percent SOPCOOH at seven temperatures: minus 3, 0, 3, 6, 9, 12, and 15 degrees Celsius. Colors range from dark blue at minus 3 degrees to dark red at 15 degrees. Two vertical dashed lines mark 440 and 490 nanometres. The emission spectra are broader and the distinction between gel-phase and fluid-phase spectral shapes is less pronounced than at lower oxidation levels. The peak near 440 nanometres is substantially reduced even at minus 3 degrees Celsius, and the 490 nanometre shoulder is relatively enhanced, indicating a more disordered gel phase. All curves are more closely spaced in intensity compared to less oxidized samples.

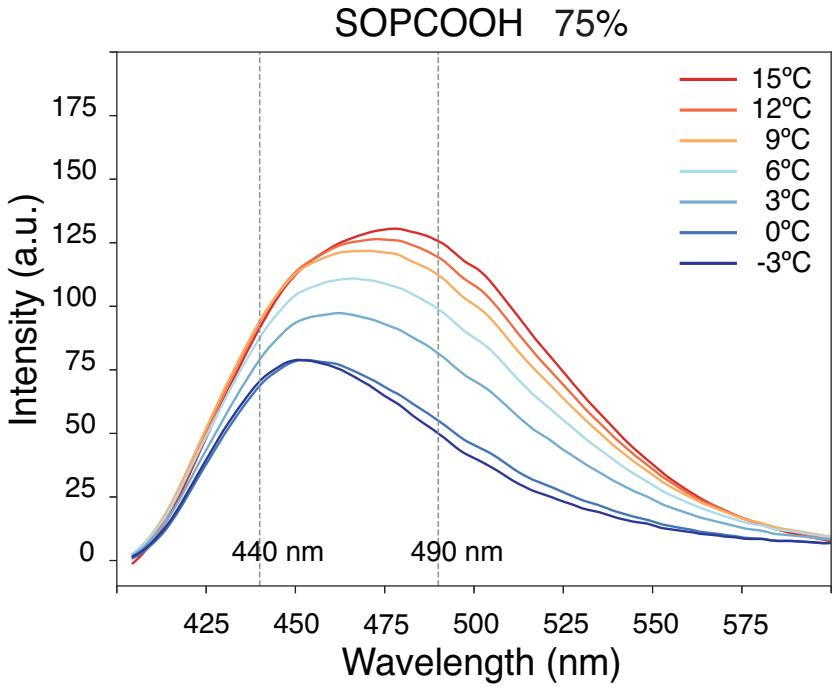

Figure S21: Laurdan emission spectra when inserted in SOPC/SOPCOOH mixtures with 75% SOPCOOH at temperatures (T) of -3, 0, 3, 6, 9, 12 and 15 °C.

Line plot showing Laurdan fluorescence emission intensity in arbitrary units on the y-axis (range 0 to 175) as a function of emission wavelength in nanometres on the x-axis (range 425 to 575) for SOPC/SOPCOOH mixtures with 75 percent SOPCOOH at seven temperatures: minus 3, 0, 3, 6, 9, 12, and 15 degrees Celsius. Colors range from dark blue at minus 3 degrees to dark red at 15 degrees. Two vertical dashed lines mark 440 and 490 nanometres. The 440 nanometre peak is further reduced relative to the 490 nanometre shoulder across all temperatures, and the overall spectral intensity is lower than at lower oxidation levels. The gel-phase and fluid-phase spectra are barely distinguishable in shape, consistent with a strongly disrupted gel phase and reduced membrane cooperativity at this oxidation level.

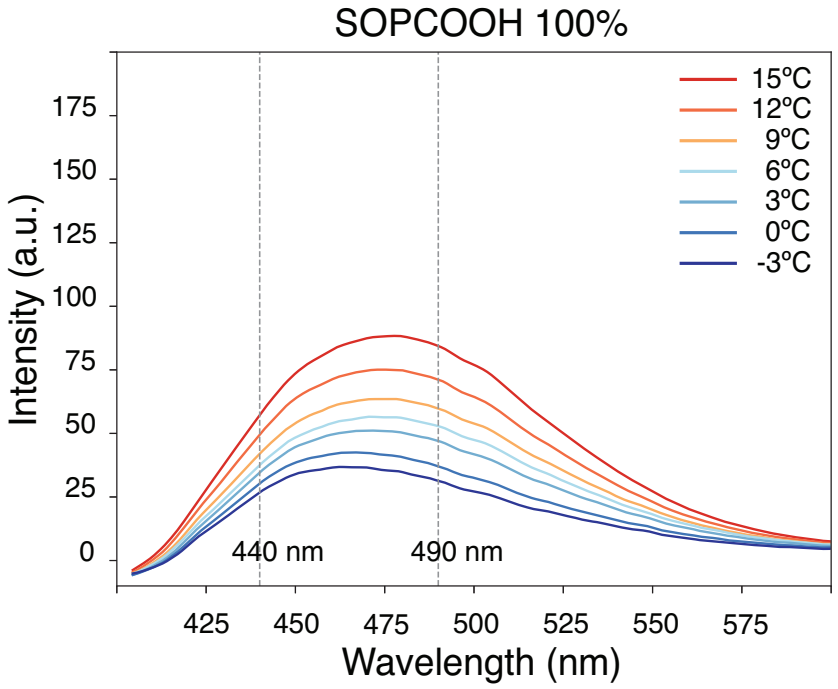

Figure S22: Laurdan emission spectra when inserted in full oxidized SOPC liposomes at temperatures (T) of -3, 0, 3, 6, 9, 12 and 15 °C.

Line plot showing Laurdan fluorescence emission intensity in arbitrary units on the y-axis (range 0 to 175) as a function of emission wavelength in nanometres on the x-axis (range 425 to 575) for fully hydroperoxidized SOPC liposomes (SOPCOOH 100 percent) at seven temperatures: minus 3, 0, 3, 6, 9, 12, and 15 degrees Celsius. Colors range from dark blue at minus 3 degrees to dark red at 15 degrees. Two vertical dashed lines mark 440 and 490 nanometres. The overall emission intensity is the lowest observed across all compositions, and all curves show a broad, featureless profile without a clear dominant peak at either 440 or 490 nanometres. The spectral shape varies little with temperature, and the emission maximum lies near or between the two reference wavelengths at all temperatures, consistent with a highly hydrated and disordered membrane environment throughout the temperature range explored.